A *Spitzer*-IRS Spectroscopic atlas of early-type galaxies in the *Revised Shapley-Ames Catalog*

R. Rampazzo[1]⋆, P.Panuzzo[2], O. Vega[3], A. Marino[4], A. Bressan[5], M.S. Clemens[1]

[1] *INAF Osservatorio Astronomico di Padova, Vicolo dell'Osservatorio 5, 35122 Padova, Italy*
[2] *GEPI, Observatoire de Paris, CNRS, Univ. Paris Diderot, Place Jules Janssen 92190 Meudon, France*
[3] *Instituto Nacional de Astrofísica, Optica y Electrónica, Apdos. Postales 51 y 216, C.P. 72000 Puebla, Pue., México*
[4] *Università degli Studi di Padova, Dipartimento di Fisica e Astronomia "G. Galilei" Vicolo dell'Osservatorio 3, 35122, Padova, Italy*
[5] *Scuola Internazionale Superiore di Studi Avanzati (SISSA), via Bonomea, 265 - 34136 Trieste ITALY*

ABSTRACT

We produce an atlas of homogeneously reduced and calibrated low resolution IRS spectra of the nuclear regions of nearby early-type galaxies (i.e. Es and S0s, ETGs), in order to build a reference sample in the mid-infrared window. From the *Spitzer* Heritage Archive we extract ETGs in the *Revised Shapley-Ames Catalog of Bright Galaxies* having an IRS SL and/or LL spectrum. We recover 91 spectra out of 363 galaxies classified as ETGs in the catalog: 56 E (E0-E6), 8 mixed E/S0+S0/E, 27 S0 (both normal and barred - SB0) plus mixed types SB0/Sa+SB0/SBa. For each galaxy, we provide the fully reduced and calibrated spectrum, the intensity of nebular and molecular emission lines as well as of the Polycyclic Aromatic Hydrocarbons (PAHs) after a template spectrum of a passively evolving ETG has been subtracted. Spectra are classified into five mid-infrared classes, ranging from AGN (class-4) and star forming nuclei (class-3), transition class-2 (with PAHs) and class-1 (no-PAHs) to passively evolving nuclei (class-0).
A *demographic* study of mid-infrared spectra shows that Es are significantly more passive than S0s: $46^{+11}_{-10}\%$ of Es and $20^{+11}_{-7}\%$ of S0s have a spectrum of class-0. Emission lines are revealed in $64^{+12}_{-6}\%$ of ETGs. The $H_2S(1)$ line is found with similar rate in Es ($34^{+10}_{-8}\%$) and in S0s ($51^{+15}_{-12}\%$). PAHs are detected in $47^{+8}_{-7}\%$ of ETGs, but only $9^{+4}_{-3}\%$ have PAHs ratios typical of star forming galaxies.
Several indicators, such as peculiar morphologies and kinematics, dust–lane irregular shape, radio and X-ray properties, suggest that mid-infrared spectral classes are connected to phases of accretion/feedback phenomena occurring in the nuclei of ETGs.

Key words: – Infrared: galaxies – galaxies: elliptical and lenticular, cD – galaxies: fundamental parameters –techniques: spectroscopic

1 INTRODUCTION

Early-type galaxies (Es and S0s, ETGs hereafter) are the most luminous and massive stellar aggregates in the local Universe and posses a multiphase, sometimes conspicuous, interstellar medium (ISM). The *Spitzer* Space Telescope Heritage Archive (SHA) offers, in the mid-infrared (MIR) window, new tools in the endeavor of deciphering the evolutionary history of nearby ETGs. Several *Spitzer*-IRS studies have been dedicated to unveil the MIR spectral characteristics of the nuclear region of ETGs, leading to the identification of Polycyclic Aromatic

Hydrocarbons (PAHs) with both normal and anomalous inter–band ratios, as well as emission lines from molecular hydrogen (Bregman et al. 2006; Bressan et al. 2006; Kaneda et al. 2005; Panuzzo et al. 2007; Kaneda et al. 2008; Panuzzo et al. 2011).

Using *Spitzer*–IRS spectra, Bressan et al. (2006) studied the nuclear properties of 20 bright ETGs in the Virgo cluster, identifying a class of *passively evolving* ETGs. Their MIR spectra are characterized by the absence of ionic and molecular emission as well as of PAHs. Only the silicate emission at $10\mu m$ from the circum–stellar dust of O-rich AGB stars leave their imprint in these spectra, superimposed on the photospheric stellar continuum generated by red giant stars (Knapp et al. 1989; Athey et al. 2002). The study of Bressan et al. (2006) also shows that ETGs with

⋆ E-mail: roberto.rampazzol@oapd.inaf.it

a passive spectrum are very common in the Virgo cluster (16 out of 20). The remaining four galaxies include already known "active" objects like NGC 4486 (M 87) and NGC 4435, the early-type companion in *The Eyes* interacting pair. Buson et al. (2009) showed that the MIR continuum of M 87 is the superposition of a passively evolving spectrum and the synchrotron emission from the central AGN. Panuzzo et al. (2007) showed that NGC 4435 has a MIR spectrum typical of star forming galaxies.

In low density environments (LDEs), the MIR spectra of ETGs show a large variety of features. In a study of 40 ETGs, mainly located in LDEs, Panuzzo et al. (2011) found that nearly 3/4 of the spectra do not show the passive characteristics found in the Virgo sample of Bressan et al. (2006). Annibali et al. (2010), using optical spectra, had already classified the activity of the ETGs in Panuzzo et al. (2011). Most of their nuclei show generic LINER characteristics, while only few are either inert/passive or AGN systems. These latter, identified in the optical using nebular line ratios through diagnostic diagrams (see Baldwin et al. 1981; Annibali et al. 2010, and reference therein), appear dominated in the MIR by hot dust emission and may show high ionization emission lines. In the MIR, several optical LINERs show star forming spectra, similar to NGC 4435, with PAH emission typical of late-type galaxies (Smith et al. 2007). Therefore, MIR spectra provide new clues for the understanding of the mechanisms that power LINERs.

Panuzzo et al. (2011) classified the MIR spectra of ETGs into a five spectral classes. The majority of the optical LINERs can be classified into three MIR classes displaying nebular and molecular emission (H_2) without PAHs or with either normal or anomalous PAHs (Bregman et al. 2006; Kaneda et al. 2005, 2007; Vega et al. 2010). Among the spectra with PAHs, the most populated class of MIR spectra (50%) shows anomalous PAH inter-band ratios ($7.7\mu m/11.3\mu m \leqslant 2.3$). The least populated class shows normal, star forming, PAH ratios.

Given the short life time of PAHs within the ISM of ETGs (Clemens et al. 2010), Panuzzo et al. (2011) proposed that MIR classes may trace the evolutionary phases of a nucleus as the result of an accretion episode. Multi-wavelength observations of the Panuzzo et al. (2011) sample support this hypothesis (Annibali et al. 2007; Marino et al. 2011; Rampazzo et al. 2011). Accretion in ETGs may be the result of either secular evolution, driven by bar resonances, interaction or minor merger episodes which may induce nuclear star formation and/or AGN activity. Such activity, fading out with time, leaves traces in emission lines, PAH emission and the underlying continuum, until the nucleus returns to a passive state. MIR spectral classes may also offer snapshots of so-called AGN feedback i.e. the interaction between the energy and radiation generated by accretion onto the massive black hole with gas in the host galaxy (Fabian 2012). AGN feedback may arise where the intense flux of photons and particles, produced by the AGN, strips the interstellar gas, halting both star formation and accretion onto the AGN itself.

Testing these hypotheses motivated us to query the *Spitzer* Archive for high S/N, low–resolution IRS spectra in the quest for a larger sample of well studied, nearby ETGs. To this end we used the *Revised Shapley-Ames Catalogue of Bright Galaxies* (RSA hereafter) (Sandage & Tammann 1987) as our starting point. RSA classifies 363 nearby galaxies as ETGs, although it is not a complete catalogue (Sandage & Tammann 1987), it is certainly representative of bright nearby galaxies. We found 91 ETGs with *Spitzer*-IRS spectra. This paper organizes this material, homogeneously reduced and calibrated. The present atlas is intended to be a window on the MIR properties of the nuclear regions of nearby ETGs and to contribute to the understanding of their evolution. A local reference sample, made of well studied ETGs, may be used to make comparisons with numerous distant sources discovered by *Spitzer-IRS* (e.g. Sargsyan et al. 2011).

The paper is organized as follows. In section 2 we present the characteristics of the *Spitzer*-IRS sample. Section 3 provides information about observations and the strategy for spectra extraction and calibration. ETG spectra are analyzed in Section 4, where we provide a measure of atomic and molecular emission lines and PAH intensities. We finally classify spectra into the MIR spectral classes devised by Panuzzo et al. (2011). In Section 5 we perform a *demographic* study of the MIR spectral classes as a function of morphological type, the galaxy environment, as well as the X-ray, CO and radio properties of the galaxies derived from the literature. In Section 6 we investigate MIR classes in the light of morphological and kinematical peculiarities widely used to infer the recent evolutionary history of ETGs.

2   THE SAMPLE

We cross match the RSA catalogue with the *Spitzer* Heritage Archive, including IRS spectra either with just SL segments or both SL and LL segments, as our priority is in characterizing spectral features and obtaining the MIR classification of the spectra as in Panuzzo et al. (2011). In Tables 1 and 2 we list the resulting sample of 91 ETGs and in Tables 3 and 4 the basic observational parameters. Although by no means complete, this atlas doubles the Panuzzo et al. (2011) sample, the largest study to date.

ETGs are divided according to their RSA morphological classification (column 2) into Es and S0s. In the S0 family we include both *bona fide* S0s, in their normal and barred forms, and the "mixed" sub-classes E/S0 and S0/E. Tables 1 and 2 also report the morphological type code, T (column 3), provided in HYPERCAT. The sample of Es is composed of 56 galaxies: different sub-classes, from E0 to E6, are all populated. The sample of S0s consists of 35 galaxies of several sub-types, including mixed cases i.e. E/S0, S0/Sa or SB0/Sa. In all cases the morphological type code, T, is $\leqslant 0$, as expected for ETGs. Most of the E galaxies have $T \leqslant -3$. Remarkable exceptions are NGC 1297 (T=-2.5 ± 0.9) and NGC 1275 ($T = -2.2\pm1.7$) classified as E-S0 and S0, respectively, in HYPERCAT. S0s in RSA span all the $T < 0$ range, consistently with their mixed nature. About 1/3 of E/S0 + S0 (see Table2) are considered truly Es ($T \leqslant -3$) in HYPERCAT.

The redshift independent distances, D, (column 4) and the absolute K-mag, M_K, (column 6) are from the Extragalactic Distance Database (Tully et al. 2009) and the effective radius, r_e (column 7), from RC3 (de Vaucouleurs et al. 1991). For galaxies, labeled with an asterisk, we use a Hubble constant of 73 km s^{-1} Mpc^{-1} and the heliocentric veloc-

Table 1. The sample of E galaxies

Ident.	Morpho. RSA	T	D [Mpc]	T88[a] Group	M_K	r_e [kpc]	σ_c [km s^{-1}]
E							
NGC 636	E1	-4.8±0.5	30	52 -7 7	-23.94	2.8	165
NGC 720	E5	-4.8±0.5	28	52 -9 7	-24.94	4.9	241
NGC 821	E6	-4.8±0.4	24*	52 0 0	-24.00	5.8	200
NGC 1209	E6	-4.5±1.0	36	51-14 14	-24.46	3.2	240
NGC 1275	E pec	-2.2±1.7	72*		-26.16	5.9	259
NGC 1297	E2	-2.5±0.9	29	51 -7 4	-23.36	4.0	115
NGC 1339	E4	-4.3±0.5	20	51 2 1	-22.78	3.9	346
NGC 1374	E0	-4.4±1.1	20	51 -1 1	-23.30	2.4	186
NGC 1379	E0	-4.8±0.5	20	51 -1 1	-23.28	4.0	120
NGC 1395	E2	-4.8±0.5	20	51 -4 4	-24.64	4.7	245
NGC 1399	E1	-4.6±0.5	21	51 -1 1	-25.30	4.1	345
NGC 1404	E2	-4.8±0.5	20	51 -1 1	-24.71	2.3	234
NGC 1407	E0	-4.5±0.7	29	51 -8 4	-25.62	9.9	286
NGC 1426	E4	-4.8±0.5	24	51 -4 4	-23.24	2.9	162
NGC 1427	E5	-4.0±0.9	20	51 -1 1	-23.33	3.0	162
NGC 1453	E2	-4.7±0.7	54		-25.57	6.5	332
NGC 1549	E2	-4.3±0.9	16*	53 -1 1	-24.24*	3.5	202
NGC 1700	E3	-4.7±0.9	44		-25.16	3.9	239
NGC 2300	E3	-3.4±1.4	26	42-16 16	-24.51	4.0	261
NGC 2974	E4	-4.2±1.2	21	31-18 18	-25.42	2.5	220
NGC 3193	E2	-4.8±0.5	34	21 -6 6	-24.69	4.0	194
NGC 3258	E1	-4.3±0.9	32	31 -2	-24.25	4.6	271
NGC 3268	E2	-4.3±0.9	35	31 -2	-24.60	6.1	227
NGC 3377	E6	-4.8±0.4	11	15 -1 1	-22.71	1.8	139
NGC 3379	E0	-4.8±0.5	11	15 -1 1	-24.04	1.9	209
NGC 3557	E3	-4.8±0.5	46	31-10 10	-26.13	6.7	265
NGC 3608	E1	-4.8±0.5	23	21 -1 1	-24.80	3.5	192
NGC 3818	E5	-4.6±0.8	36	22 -8 8	-23.95	3.8	191
NGC 3904	E2	-4.7±0.6	28	22 -4 4	-24.61	3.3	205
NGC 3962	E1	-4.8±0.4	35	22 1 1	-25.09	6.0	225
NGC 4261	E3	-4.8±0.4	32	11-24 24	-25.24	5.6	309
NGC 4365	E3	-4.8±0.5	23	11 -5 1	-25.19	5.6	256
NGC 4374	E1	-4.3±1.2	19	11 -1 1	-25.13	4.7	282
NGC 4473	E5	-4.7±0.7	15	11 -1 1	-23.77	1.9	179
NGC 4478	E2	-4.8±0.4	20*	11 -1 1	-23.15*	1.3	137
NGC 4486	E0	-4.3±0.6	17	11 -1 1	-25.81	7.8	334
NGC 4564	E6	-4.8±0.5	16	11 -1 1	-23.09	1.5	157
NGC 4589	E2	-4.8±0.4	22	42-13 13	-23.96	1.4	224
NGC 4621	E5	-4.8±0.5	15	11 -1 1	-24.13	2.9	225
NGC 4660	E5	-4.7±0.5	15	11 -1 1	-22.69	0.9	203
NGC 4696	E3	-3.8±0.6	18*	23 -1 1	-24.13*	7.4	254
NGC 4697	E6	-4.4±0.8	13	11-11 10	-24.13	4.5	174
NGC 5011	E2	-4.8±0.5	42*	23 0 2	-24.97*	4.8	249
NGC 5018	E4	-4.4±1.0	38	11 0 0	-25.23	4.2	209
NGC 5044	E0	-4.8±0.4	31	11-31 31	-24.79	12.4	239
NGC 5077	E3	-4.8±0.4	39	11 0 0	-24.73	4.3	260
NGC 5090	E2	-4.9±0.3	47*	23 0 2	-25.79*	14.2	269
NGC 5638	E1	-4.8±0.4	26	41 -3 1	-23.86	3.5	165
NGC 5812	E0	-4.8±0.4	27	41 0 1	-24.22	3.3	200
NGC 5813	E1	-4.8±0.4	32	41 -1 1	-25.15	8.9	239
NGC 5831	E4	-4.8±0.5	27	41 -1 1	-23.75	3.3	164
NGC 7619	E3	-4.7±0.6	53		-25.62	9.5	322
IC 1459	E1	-4.8±0.6	29	61-17 16	-25.53	4.8	311
IC 2006	E1	-4.2±0.9	20	51 -1 1	-23.05	2.8	122
IC 3370	E2 pec	-4.8±0.5	27	23 0 5	-24.32	5.1	202
IC 4296	E0	-4.8±0.4	52		-26.09	10.4	340

[a] The group/cluster identification (Tully 1988, T88) is the following: 11 Virgo cluster and Southern Extension, 12 Ursa Major Cloud, 13 Ursa Major Southern Spur, 14 Coma–Sculptor Cloud, 15 Leo Spur, 21 Leo Cloud, 22 Crater cloud, 23 Centaurus Cloud, 31 Antlia – Hydra Cloud, 41 Virgo – Libra Cloud, 42 Canes Venatici, 43 Canes Venatici Spur, 44 Draco Cloud, 51 Fornax and Eridanus Cloud, 52 Cetus – Aries Cloud, 53 Dorado Cloud, 61 Telescopium – Grus Cloud, 62 Pavo – Indus Spur, 65 Pegasus Spur.

Table 2. The sample of E/S0, S0 and SB0 galaxies

Ident.	Morpho. RSA	T	D [Mpc]	T88[a] Group	M_K	r_e [kpc]	σ_c [km s^{-1}]
E/S0 and S0/E							
NGC 1052	E3/S0	-4.6±0.8	19	52 -1 1	-24.00	3.1	215
NGC 1351	S0$_1$(6)/E6	-3.1±0.6	19	51 -1 1	-22.64	1.9	140
NGC 4472	E1/S0$_1$(1)	-4.8±0.5	17	11 -1 1	-25.73	8.2	294
NGC 4550	E7/S0$_1$(7)	-2.1±0.7	15	11 -1 1	-22.25	1.1	96
NGC 4570	S0$_1$(7)/E7	-2.0±0.7	17	11 -1 1	-23.49	1.5	188
NGC 4636	E0/S0$_1$(6)	-4.8±0.5	15	11 2 1	-24.42	6.4	209
NGC 5353	S0$_1$(7)/E7	-2.1±0.6	30	42 -1 1	-24.74	2.1	286
NGC 6868	E3/S0$_{2/3}$(3)	-4.8±0.6	38*	61 -1 1	-25.58*	6.2	277
S0,SB0,S0/Sa,SB0/Sa							
NGC 584	S0$_1$(3,5)	-4.6±0.9	20	52 -7 7	-24.23	2.4	206
NGC 1366	S0$_1$(8)	-2.3±0.7	17*	51 2 1	-22.14*	0.9	120
NGC 1389	S0$_1$(5)/SB0$_1$	-2.8±0.7	21	51 -1 1	-23.00	1.5	139
NGC 1533	SB0$_2$(2)/SBa	-2.5±0.6	11*	53 -1 1	-22.58*	1.6	174
NGC 1553	S0$_{1/2}$ pec	-2.3±0.6	18*	53 -1 1	-25.00*	5.7	180
NGC 2685	S0$_3$(7) pec	-1.0±0.8	12	13 -4 4	-22.08	1.9	94
NGC 3245	S0$_1$	-2.1±0.5	21	21 -8 8	-23.75	2.7	210
NGC 4036	S0$_3$(8)/Sa	-2.6±0.7	20	12 -5 1	-23.93	3.0	189
NGC 4339	S0$_{1/2}$(0)	-4.7±0.8	16	11 4 1	-22.55	2.5	114
NGC 4371	SB0$_{2/3}$(r)(3)	-1.3±0.6	17	11 -1 1	-23.44	1.9	135
NGC 4377	S0$_1$(3)	-2.6±0.6	18	11 -1 1	-22.43	1.1	144
NGC 4382	S0$_1$(3) pec	-1.3±0.6	18	11 -1 1	-25.13	4.8	178
NGC 4383	S0	-1.0±0.5	22*	11 -1 1	-22.22*	1.2	...
NGC 4435	SB0$_1$(7)	-2.1±0.5	12*	11 -1 1	-23.10*	1.2	157
NGC 4442	SB0$_1$(6)	-1.9±0.4	15	11 -1 1	-23.63	1.8	187
NGC 4474	S0$_1$(8)	-2.0±0.5	15	11 -1 1	-22.27	1.5	88
NGC 4477	SB0$_{1/2}$/SBa	-1.9±0.4	19	11 -1 1	-24.06	3.5	186
NGC 4552	S0$_1$(0)	-4.6±0.9	16	11 -1 1	-24.31	2.3	264
NGC 4649	S0$_1$(2)	-4.6±0.8	16	11 -1 1	-25.35	5.3	335
NGC 5128	S0+S pec	-2.1±0.6	7*	14-15 15	-25.28*		120
NGC 5273	S0/a	-1.9±0.4	17	43 1 1	-22.43	2.5	66
NGC 5631	S0$_3$(2)/Sa	-1.9±0.4	28	42 -7 3	-23.76	2.6	171
NGC 5846	S0$_1$(0)	-4.7±0.7	25	41 -1 1	-25.07	7.6	250
NGC 5898	S0$_{2/3}$(0)	-4.3±0.9	29	41-11 11	-24.31	3.1	220
NGC 7192	S0$_2$(0)	-3.9±0.7	38*	62 -2 1	-24.39*	5.3	257
NGC 7332	S0$_{2/3}$	-1.9±0.5	23	65 -2 1	-23.81	1.6	136
IC 5063	S0$_3$(3) pec/Sa	-1.1±0.5	47*		-24.61*	6.1	160

[a] As in Table 1.

ity, V_{hel}, from NED. Most of the galaxies in the sample have a heliocentric systemic velocity lower than 3500 km s^{-1}. Only NGC 1275, NGC 1453, NGC 1700, NGC 7619 and IC 4296 exceed this limit. In the global sample, distances of the galaxies are less than 72 Mpc. For each galaxy we report the cluster/group association to which the galaxy should be gravitationally bound (see column 5 and the note of Table 1). These data are provided in the T3000 catalogue (Tully et al. 2009). Es and S0s are located in different environments. Our sample includes 31 cluster members, 21 located in the denser regions of Virgo (T88 group 11 -1 1, 11 +2 +1) and 8 of Fornax (T88 group 51 -1 1) clusters. According to Tully (1988), the environmental density associated with cluster members is $\rho \geqslant 1.33$ (gal Mpc^{-3}). Two additional galaxies, NGC 1275 (Perseus cluster), NGC 7619 (Pegasus I cluster), too distant to be found in Tully's Catalogue, have been included in the present cluster sample. The remaining 60 ETGs are located in LDEs and have $\rho \leqslant 0.97$ (gal Mpc^{-3}).

Our sample of Es and S0s presents fundamental char-

acteristics noticed in different samples. In Tables 1 and 2 we report the M_{K_T} (column 6), a proxy of the stellar mass, and the central velocity dispersion (column 8), σ_c, (from HYPERCAT) a proxy of the total galaxy mass (Clemens et al. 2006, 2009). We applied a Mann-Whitney U-Test (Wall 1977) to both the M_{K_T} and σ_c distributions of Es and of S0s to compare the properties of the two samples. We verified the null hypothesis that the two samples result from the same parent population can be rejected at the 99% confidence level. The median of M_{K_T} and of σ_c distributions for Es is larger than those of S0s, suggesting that Es are less dominated by Dark Matter than S0s of similar total mass. Shankar et al. (2004, their Figure 1) noticed that the different dominance of Dark Matter in Es with respect to S0s suggest that the two morphological families had different evolution mechanisms.

Table 3. The *Spitzer*–IRS observations of E galaxies in RSA

ident	PI	ID	SL1 [s×Cycle]	SL2 [s×Cycle]	LL2 [s×Cycle]	LL1 [s×Cycle]	slit [3.6"×18"] [kpc×kpc]	Area$_{slit}$/Area$_{r_e/8}$
E								
NGC 636	Bregman	3535	14×8	14×8	30×6	...	0.5×2.6	3.5
NGC 720	Bregman	3535	14×8	14×8	30×6	...	0.5×2.4	1.0
NGC 821	Bregman	3535	14×8	14×8	30×6	...	0.4×2.1	0.5
NGC 1209	Rampazzo	30256	60×6	60×6	120×16	120×8	0.6×3.1	3.9
NGC 1275	Houck	14	14×2	14×2	6×4	6×4	1.3×6.3	4.6
NGC 1297	Rampazzo	30256	60×19	60×19	120×14	120×8	0.5×2.5	1.6
NGC 1339	Bregman	3535	14×8	14×8	30×6	..	0.3×1.7	0.8
NGC 1374	Bregman	3535	14×8	14×8	30×6	...	0.3×1.7	2.2
NGC 1379	Bregman	3535	14×8	14×8	30×6	...	0.3×1.7	0.8
NGC 1395	Kaneda	3619/30483	60×2	60×2	30×2	30×2	0.3×1.7	0.6
NGC 1399	Bregman	3535	14×8	14×8	30×6	...	0.3×1.7	0.8
NGC 1404	Bregman	3535	14×8	14×8	30×6	...	0.4×1.8	2.3
NGC 1407	Kaneda	3619/30483	60×2	60×2	30×2	30×2	0.5×2.5	0.3
NGC 1426	Rampazzo	30256	60×12	60×12	120×14	120×8	0.4×2.1	2.1
NGC 1427	Bregman	3535	14×8	14×8	30×6	...	0.3×1.7	1.4
NGC 1453	Bregman	3535	14×8	14×8	30×6	...	0.9×4.7	2.1
NGC 1549	Kaneda	30483	60×4	60×4	30×4	30×4	0.3×1.4	0.6
NGC 1700	Bregman	3535	14×8	14×8	30×6	...	0.8×3.8	3.8
NGC 2300	Bregman	3535	14×8	14×8	30×6	...	0.4×2.3	1.3
NGC 2974	Kaneda	3619/30483	60×2	60×2	30×3	30×3	0.4×1.8	2.2
NGC 3193	Appleton	50764	14×4	14×3	30×2	30×2	0.6×3.0	2.2
NGC 3258	Rampazzo	30256	60×8	60×8	120×14	120×8	0.6×2.8	1.4
NGC 3268	Rampazzo	30256	60×9	60×9	120×14	120×8	0.6×3.0	1.0
NGC 3377	Bregman	3535	14×8	14×8	30×6	...	0.2×1.0	1.1
NGC 3379	Bregman	3535	14×8	14×8	30×6	...	0.2×1.0	1.1
NGC 3557	Kaneda	30483	60×3	60×3	30×3	30×3	0.8×4.0	1.5
NGC 3608	Bregman	3535	14×8	14×8	30×6	...	0.4×2.0	1.3
NGC 3818	Rampazzo	30256	60×19	60×19	120×14	120×8	0.6×3.1	2.7
NGC 3904	Kaneda	30483	60×3	60×3	30×4	30×4	0.5×2.4	2.2
NGC 3962	Kaneda	3619/30483	60×2	60×2	30×3	30×3	0.6×3.0	1.1
NGC 4261	Antonucci	20525	240×2	240×3	120×3	120×2	0.6×2.8	1.0
NGC 4365	Bressan	3419	60×3	60×3	120×3	...	0.4×2.0	0.5
NGC 4374	Rieke	82	60×4	60×4	120×4	120×4	0.3×1.7	0.5
NGC 4473	Bressan	3419	60×3	60×3	120×3	...	0.3×1.3	1.9
NGC 4478	Bregman	3535	14×8	14×8	30×6	...	0.3×1.7	7.3
NGC 4486	Bressan	3419	60×3	60×3	120×3	...	0.3×1.5	0.1
NGC 4564	Bressan	3419	60×4	60×4	120×6	...	0.3×1.4	3.3
NGC 4589	Kaneda	3619/30483	60×2	60×2	30×2	30×2	0.4×1.9	7.9
NGC 4621	Bressan	3419	60×3	60×3	120×3	...	0.3×1.3	0.8
NGC 4660	Bressan	3419	60×3	60×3	120×5	...	0.3×1.3	8.8
NGC 4696	Kaneda	3619/30483	60×2	60×2	30×3	30×3	0.3×1.6	0.2
NGC 4697	Bregman	3535	14×8	14×8	30×6	...	0.2×1.1	0.3
NGC 5011	Rampazzo	30256	60×6	60×6	120×12	120×8	0.7×3.7	2.3
NGC 5018	Kaneda	30483	60×4	60×4	30×3	30×3	0.7×3.3	2.5
NGC 5044	Rampazzo	30256	19	19	14	8	0.5×2.7	0.2
NGC 5077	Rampazzo	30256	60×12	60×12	120×14	120×8	0.7×3.4	2.5
NGC 5090	Kaneda	30483	60×4	60×4	30×3	30×3	0.8×4.1	0.3
NGC 5638	Bregman	3535	14×8	14×8	30×6	...	0.4×2.3	1.7
NGC 5812	Bregman	3535	60×6	60×6	120×12	120×8	0.5×2.4	2.0
NGC 5813	Bregman	3535	14×8	14×8	30×6	...	0.6×2.8	0.4
NGC 5831	Bregman	3535	14×8	14×8	30×6	...	0.5×2.4	2.0
NGC 7619	Bregman	3535	14×8	14×8	30×6	...	0.9×4.6	1.0
IC 1459	Kaneda	30483	60×3	60×3	30×2	30×2	0.5×2.5	1.1
IC 2006	Bregman	3535	14×8	14×8	30×6	...	0.3×1.7	1.6
IC 3370	Kaneda	3619/30483	60×2	60×2	30×3	30×3	0.5×2.4	0.9
IC 4296	Antonucci	20525	240×2	240×2	120×3	120×3	0.9×4.5	0.8

Table 4. The *Spitzer*–IRS observations of E/S0s and S0s in RSA

ident	PI	ID	SL1 [s×Cycle]	SL2 [s×Cycle]	LL2 [s×Cycle]	LL1 [s×Cycle]	slit [3.6"×18"] [kpc×kpc]	$Area_{slit}/Area_{r_e/8}$
E/S0 and S0/E								
NGC 1052	Kaneda	30483	60×2	60×2	30×2	30×2	0.3×1.7	1.2
NGC 1351	Bregman	3535	14×8	14×8	30×6	...	0.3×1.7	3.2
NGC 4472	Bregman	3535	14×8	14×8	30×6	...	0.3×1.5	0.1
NGC 4550	Bressan	3419	60×20	60×20	120×14	...	0.3×1.3	5.8
NGC 4570	Bressan	3419	60×3	60×3	120×5	...	0.3×1.5	4.2
NGC 4636	Bressan	3419	60×3	60×3	120×5	...	0.2×1.3	0.2
NGC 5353	Appleton	50764	60×1	60×1	30×2	30×2	0.5×2.6	6.1
NGC 6868	Rampazzo	30256	60×6	60×6	120×13	120×8	0.7×3.3	1.2
S0,SB0,S0/Sa,SB0/Sa								
NGC 584	Bregman	3535	14×8	14×8	30×6	...	0.3×1.7	2.1
NGC 1366	Rampazzo	30256	60×11	60×11	120×14	120×8	0.3×1.5	11.7
NGC 1389	Rampazzo	30256	60×9	60×9	120×14	120×8	0.4×1.8	5.8
NGC 1533	Rampazzo	30256	60×3	60×3	120×5	120×3	0.2×1.0	1.5
NGC 1553	Rampazzo	30256	60×3	60×3	120×3	120×3	0.3×1.6	0.3
NGC 2685	Rieke	40936	14×6	14×6	14×6	14×6	0.2×1.0	1.3
NGC 3245	Sturm	3237	14×2	14×2	...	...	0.3×1.8	1.8
NGC 4036	Sturm	3237	14×2	14×2	...	...	0.3×1.7	1.4
NGC 4339	Bressan	3419	60×20	60×20	120×14	...	0.3×1.4	1.3
NGC 4371	Bressan	3419	60×9	60×9	120×10	...	0.3×1.5	2.4
NGC 4377	Bressan	3419	60×12	60×12	120×8	...	0.3×1.6	7.7
NGC 4382	Bressan	3419	60×3	60×3	120×3	...	0.3×1.6	0.4
NGC 4383	Weedman	50834	60×2	60×2	120×1	120×1	0.4×1.9	10.5
NGC 4435	Bressan	3419	60×3	60×3	120×5	...	0.2×1.0	3.1
NGC 4442	Bressan	3419	60×3	60×3	120×3	...	0.3×1.3	2.2
NGC 4474	Bressan	3419	60×20	60×20	120×24	...	0.3×1.3	3.1
NGC 4477	Riecke	40936	14×6	14×6	14×6	14×6	0.3×1.7	0.9
NGC 4552	Bregman	3535	14×8	14×8	30×6	...	0.3×1.4	1.5
NGC 4649	Bregman	3535	14×8	14×8	30×6	...	0.3×1.4	0.3
NGC 5128	Houck/Lacy	14	6×4/6×4	6×4/6×4	6×4	6×4	0.1×0.6	
NGC 5273	Riecke	40936	6×2		6×2	6×2	0.3×1.5	1.4
NGC 5631	Riecke	40936	14×6	14×6	14×6	14×6	0.5×2.4	3.7
NGC 5846	Bregman	3535	14×8	14×8	30×6	...	0.4×2.2	0.3
NGC 5898	Rampazzo	30256	60×11	60×11	120×14	120×8	0.5×2.5	2.7
NGC 7192	Rampazzo	30256	60×12	60×12	120×14	120×8	0.7×3.3	1.6
NGC 7332	Rampazzo	30256	60×7	60×7	120×14	120×8	0.4×2.0	6.1
IC 5063	Gorjan	30572	14×2	14×2	30×1	30×1	0.8×4.1	1.8

3 OBSERVATIONS AND DATA REDUCTION

The details of the *Spitzer*-IRS observations for each galaxy are provided in Tables 3 and 4 for Es and S0s, respectively. In column 8 we provide the slit aperture in kpc. In column 9, the ratio between the area covered by the slit and the circular aperture of radius $r_e/8$ is given. Although we used a fixed aperture for the extraction of the spectra, the slit covers central portions of the ETGs, with a size, on the average, of about 2-3 × $\pi(r_e/8)^2$ (1.9±1.8 for Es and 2.9±2.8 for S0s). We refer to this portion as the "nuclear" part of the galaxy throughout the paper.

Observations were performed in Standard Staring mode with low resolution ($R \sim 64$–128) modules SL1 (7.4–14.5μm), SL2 (5–8.7μm), LL2 (14.1–21.3μm) and LL1 (19.5–38μm). Observations do not include, in general, all IRS modules.

The data reduction procedure is fully described in Panuzzo et al. (2011). Briefly in the following we recall the main steps of the reduction. After the removal of bad pixels from the co-added images, the sky background was re-moved by subtracting co-added images taken with the source placed in different orders at the same nod position. Offset exposures, if available, were used to measure the sky background without contamination from the target galaxy itself. For those galaxies for which only the LL2 module was used, the background subtraction was done by subtracting co–added images taken with the source at different nod positions.

In order to derive calibrated spectral energy distributions, we taken into account that the galaxies are extended, compared to the IRS point spread function (PSF). Since the IRS spectra are calibrated on point-sources, we have devised an *ad hoc* procedure to correct for the effects of the variation with wavelength of the IRS PSF. We simulated the effect of convolving an intrinsic surface brightness profile (a modified King law, Elson et al. (1987)) with the instrumental PSF, and of the extraction in a fixed width of 3.6″. This provides us a correction factor to be applied to the extracted spectrum as a function of the wavelength and the profile parameters. By fitting the observed profiles with the simulated ones, we can reconstruct the intrinsic profiles and correct the
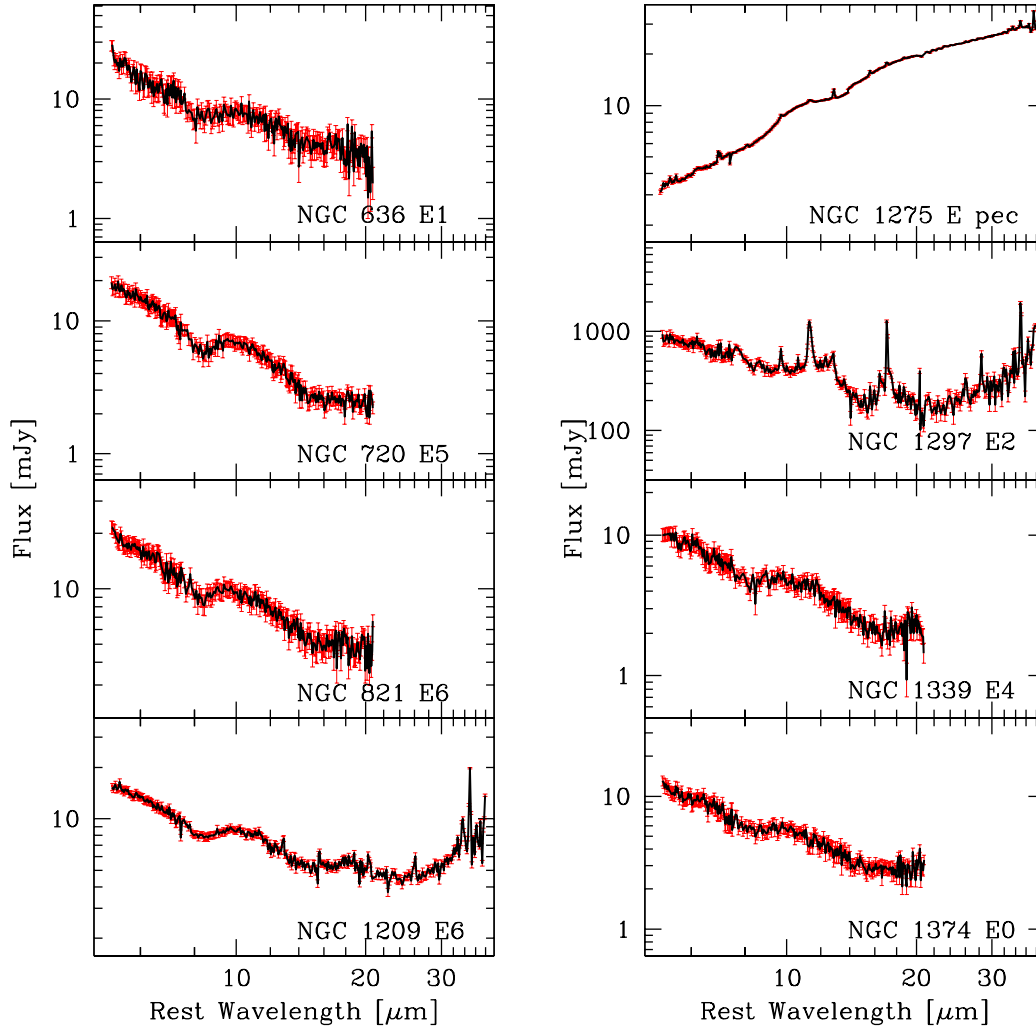
Figure 1. Spectra of Es. Flux vs. rest wavelength as obtained from Spitzer-IRS low resolution modules. Bars represent 1σ error. The LL modules have been scaled to match the SL fluxes.

extracted spectra to correspond to the intrinsic SED. This procedure also has the advantage of determining whether a particular feature is spatially extended or not.

This procedure was applied to SL modules but not to LL modules where the PSF is too large to determine the intrinsic surface brightness profile. For this reason, the spectra in the LL range are extracted as if the sources were point-like and then manually scaled to match the SL segment. This is equivalent in assuming that the light distribution at LL wavelengths is the same as that at the end of the SL segment. Note that for those sources that are fully dominated by the nucleus (i.e. AGN-dominated like NGC 1275) there is no need to rescale the LL spectra.

The rest frame, flux calibrated, IRS spectra of the sample galaxies are shown in Figure 1.

4 SPECTRAL PROPERTIES OF THE ATLAS

The present atlas aims to build, from homogeneously reduced Spitzer-IRS spectra, a data-set of emission lines and PAH intensities as well as to divide nearby ETG nuclei into MIR physical classes as in Panuzzo et al. (2011).

4.1 Analysis of MIR spectra

To analyze spectra we adopted a model of the MIR emission that takes into account the following components: 1) the underlying stellar continuum due to the old population characteristic of a passively evolving ETG includes the contribution of the dusty AGB stars which dominate the emission at wavelengths $\leqslant 6\ \mu$m (Bressan et al. 2006); 2) a featureless thermal continuum representing a putative dust contribution at longer wavelengths; 3) the emission from molecular and atomic lines and 4) the PAH features. The best fit of
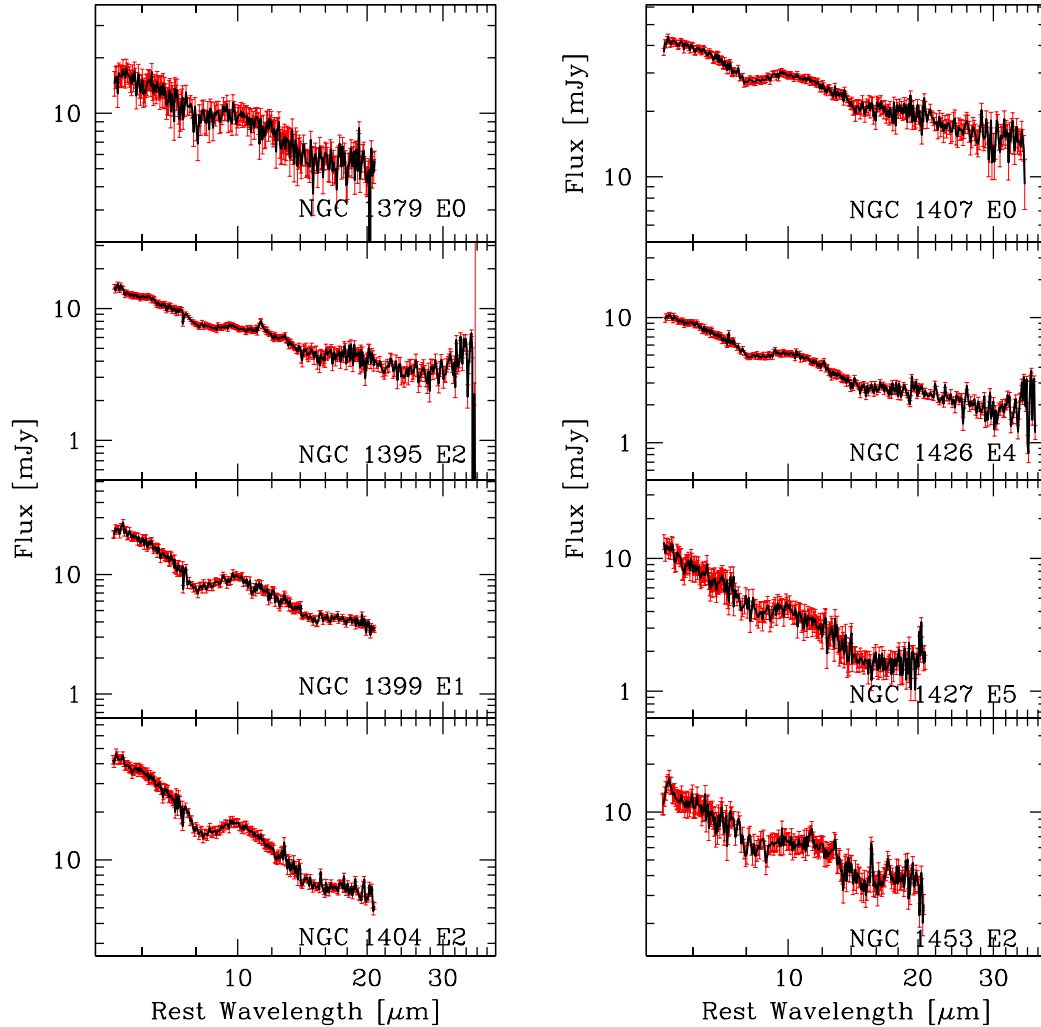
Figure 1. *(cont.)* MIR spectra of Es.

each spectrum is obtained using the Levenberg-Marquardt algorithm.

The model is fully described in Vega et al. (2010) and Panuzzo et al. (2011) and is similar to that used by Smith et al. (2007). The main difference consists in the selection of the underlying stellar continuum component. The stellar component is described by Smith et al. (2007) as the emission of a blackbody at 5000 K. This approximation, suitable for the analysis of star-forming galaxies, where the hot dust and PAH features dominate the MIR emission, is not adequate for ETGs. In these galaxies, the underlying stellar component usually dominates the MIR continuum at shorter wavelengths, and the MIR emission is characterized by a dip at 8 μm, likely due to photospheric SiO absorption bands (Verhoelst et al. 2009), and a bump at $\sim$10 μm from the silicate emission from the dusty circumstellar envelopes of O-rich AGB stars (e.g. Bressan et al. 1998, Bressan et al. 2006). We therefore adopt a semi-empirical, high S/N template derived from the analysis of passive ETGs in Panuzzo et al.

(2011) to describe the stellar continuum. The template is built by averaging the NIR (J-H-K 2MASS) data, within the central 5" radius, and the 5–40 μm *Spitzer*-IRS spectra of three passively evolving ETGs, namely NGC 1389, NGC 1426, and NGC 3818. The subtraction of the underlying stellar continuum is performed by assuming that the NIR fluxes are completely due to the stellar component. Thus, we normalize our stellar continuum template to the observed flux in the H-band, and calculate the contribution of the stellar continuum to the MIR spectra. Figure 2 provides some examples of the MIR continuum in different type of spectra and Figure 3 shows some examples of the fitting procedure (see also next section).

Measurements of PAH features and of the nebular and molecular emission lines are collected in Tables A1 and A2, respectively.
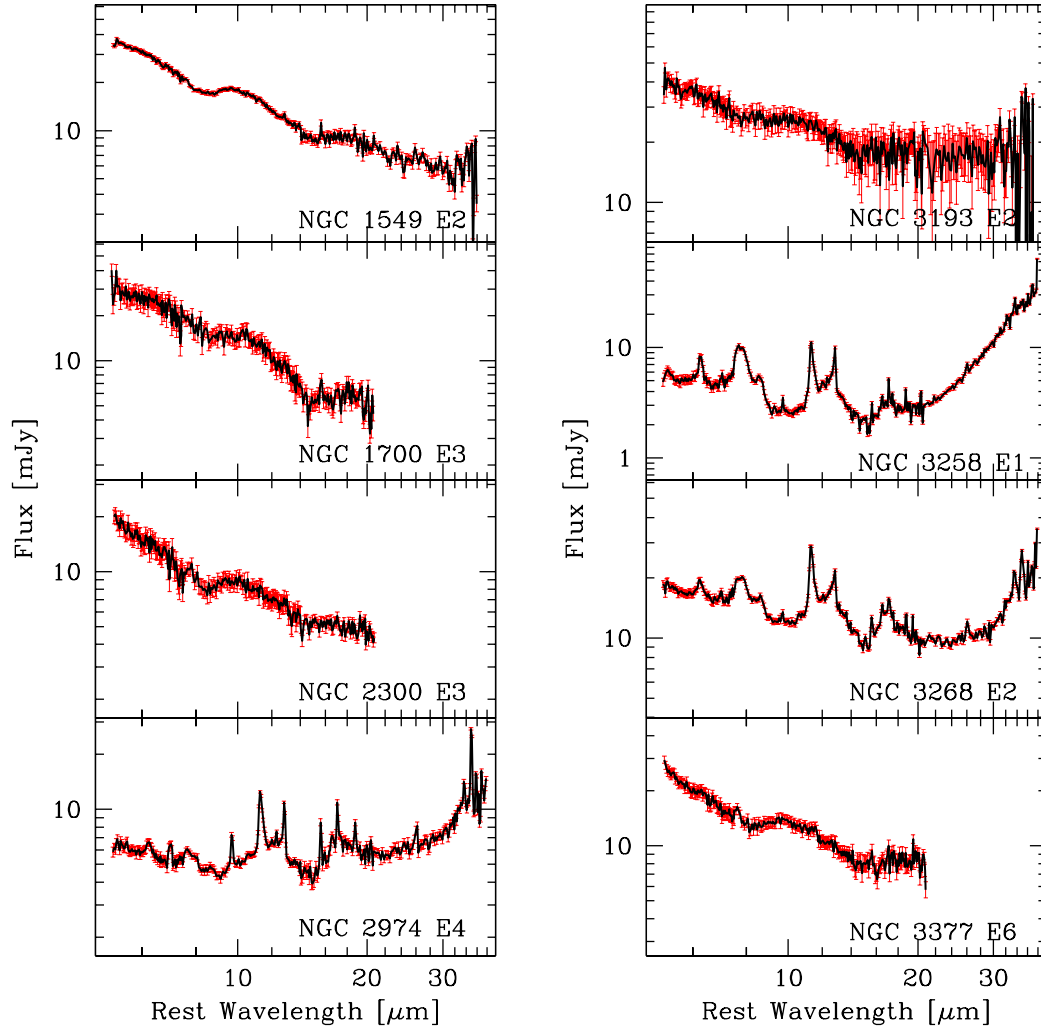
Figure 1. *(cont.)* MIR spectra of Es.

4.2 MIR spectral classes

Panuzzo et al. (2011) subdivided low resolution *Spitzer*-IRS spectra into five classes, from class-0 to class-4. Class-0 defines passively evolving nuclei. Classes from 1 to 4 aim to categorize spectra related to different powering mechanism active in the nuclear regions. The classification scheme is based on (1) the detection of emission (atomic and/or molecular) lines and PAH features, (2) the value of the PAH inter-band ratios, (3) the presence of an excess in the MIR continuum over the underlying old stellar population.

We briefly resume below the classification criteria of Panuzzo et al. (2011). Class-0 spectra show neither ionic, molecular nor PAH emission lines superimposed to the photospheric stellar continuum generated by red giant stars. Only the silicate features at ≈ 10 μm (Bressan et al. 2006) and at 18 μm (Panuzzo et al. 2011), arising from the circumstellar dust of O-rich AGB stars (Bressan et al. 1998), are present in these spectra.

Class-1 spectra show either nebular or molecular emission lines but no PAHs. Ionic, in particular [Ne II]12.8μm, [Ne III] 15.5μm, [SIII] 18.7μm, 33.5μm and molecular H_2 0-0 rotational emission lines (S(n)) are detected. The continuum of this class is similar to that of passive class-0 ETGs, at least up to 25 μm, showing, in some cases, dust emission at longer wavelengths.

All other classes show PAH complexes plus gas, ionic and molecular, emission lines. These latter include forbidden nebular emission lines of several elements like Ar, Fe, N, O, S and Si. PAH emission features are typically detected at 6.2, 7.7, 8.6, 11.3, 12.7 and 17 μm (Bregman et al. 2006; Bressan et al. 2006; Kaneda et al. 2005; Panuzzo et al. 2007; Kaneda et al. 2008; Panuzzo et al. 2011).

Classes 2 and 3 are distinguished via their different PAH inter-band ratios. Class-2 spectra have an anomalous PAH inter-band ratio, 7.7μm/11.3μm $\leqslant 2.3$. We set this value as the lower limit for the class-3 since, in their figure 14, Smith et al. (2007) show that some HII dominated sources and star-forming galaxies may reach this low PAH inter-
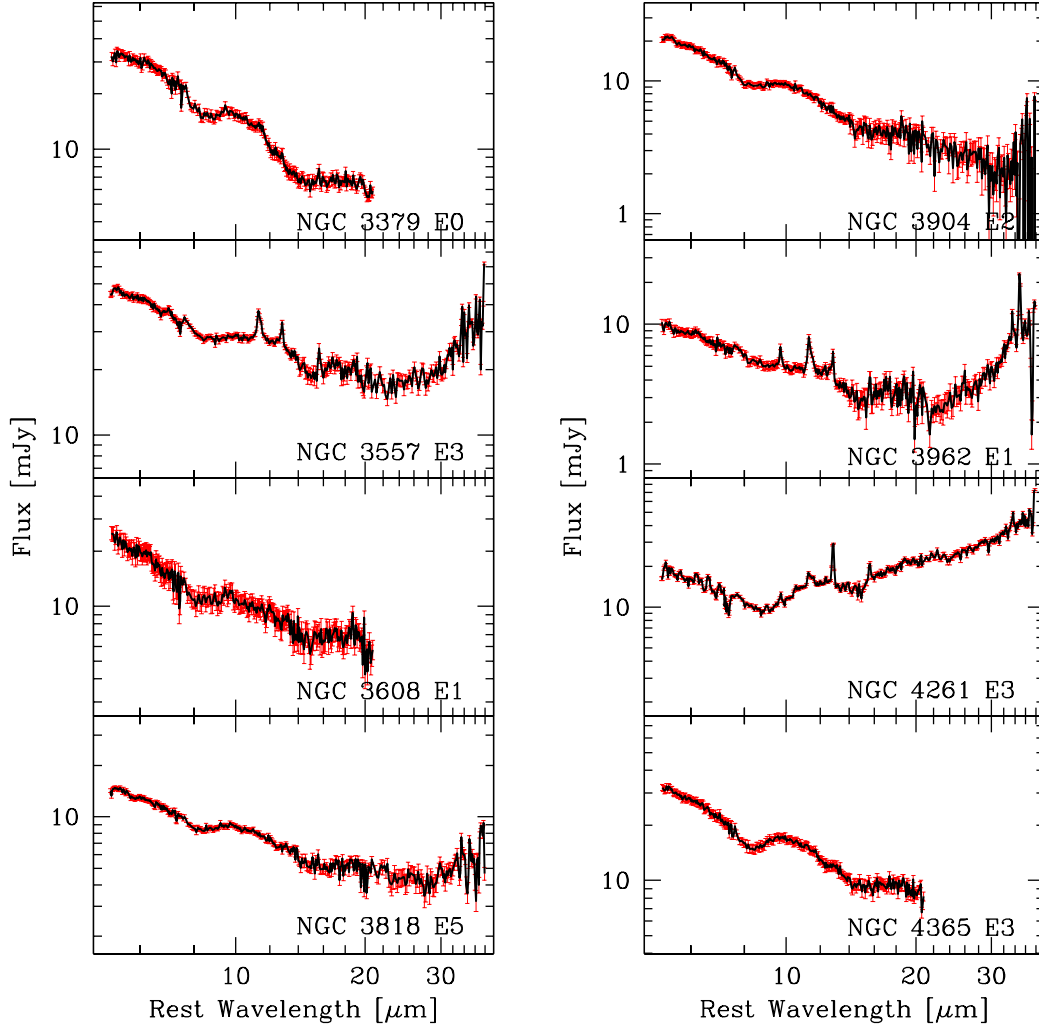
Figure 1. *(cont.)* MIR spectra of Es.

band ratio. Class-3 spectra are dominated by the 7.7μm, 11.3μm, 12.7μm and 17μm PAH complexes and have normal PAH inter-band ratios typical of star forming galaxies (Smith et al. 2007).

Finally, spectra dominated by a hot dust continuum are collected in the MIR class-4 (see discussion below). Emission lines with high ionization like [S IV] and [Ne V] and PAH features may sometimes be visible.

Figure 2 illustrates the variation of the continuum in the different MIR classes. The presence of emission lines, starts from class-1, and the importance of PAH features increases from class 2 to 3. Detailed fits of line and PAH emission features are shown in Figure 3 for NGC-4477 (class-2, top panel), NGC 5018 (class-3, mid panel) and NGC 1052 (class-4, bottom panel).

The contribution of the old stellar population to the MIR continuum decreases from class 0 to class 3, becoming almost negligible in class-4. Figure 4 shows ETGs in the color-color 2MASS J-band/6μm vs. 6μm/15μm plane, which

considers the MIR excess over the underlying old stellar population due to the hot dust. ETG nuclei of classes 3 and 4 are clearly separated from more quiescent ones (classes 0 and 1) and partly from class-2 nuclei. More quiescent ETGs are all located within a region (the rectangle in the top panel of Figure 4) delimited by old Single Stellar Population (SSP) models (age: $10 - 14.5$ Gyr and metallicity $0.004 \leqslant$ Z $\leqslant 0.05$ i.e. $\approx 1/4$ - 3 Z$_\odot$ (Bressan et al. 1998)). The 6μm/15μm value of NGC 4261 sets our empirical upper limit of class-4 ETGs. This value of the MIR excess is comparable, within errors, to NGC 4486 for which Buson et al. (2009) show that the MIR continuum is just the superposition of a passively evolving spectrum and a synchrotron emission from the central AGN.

The bottom panel of Figure 4 shows the discrimination offered by 7.7μm/11.3μm PAH ratio in disentangling active MIR classes 2, 3 and 4. All class-2 nuclei have anomalous 7.7μm/11.3μm PAH ratios and 6μm/15μm values higher than NGC 4261. All, but one, class-3 ETGs are located in the typical star burst (SB) region (solid horizon-
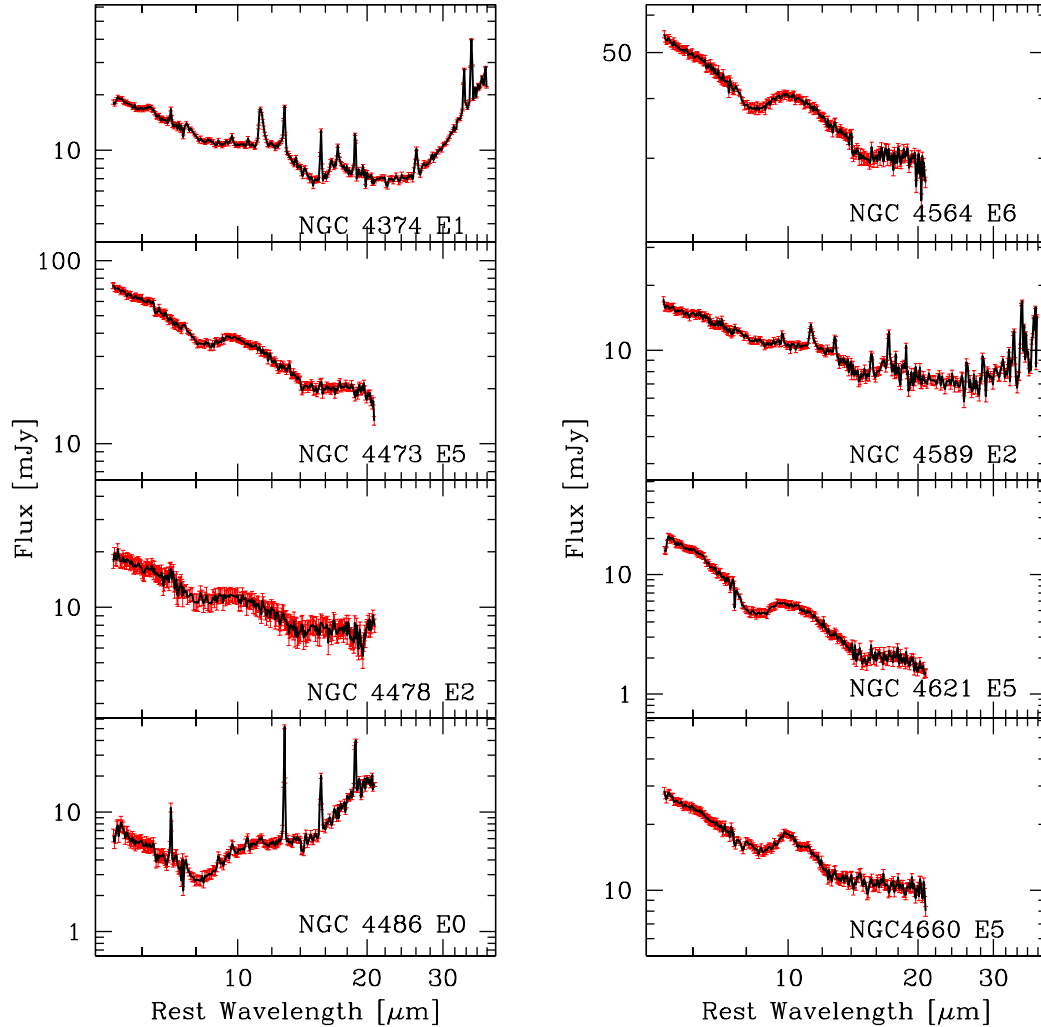
Figure 1. *(cont.)* MIR spectra of Es.

tal lines) (Smith et al. 2007). NGC 3268 is borderline between class-3 and class-2 since its $7.7\mu m/11.3\mu m$ PAH ratio $= 2.3$. NGC 5128 has both a high $6\mu m/15\mu m$ excess and a $7.7\mu m/11.3\mu m$ PAH ratio typical of star forming galaxies (see next section).

The result of our MIR spectral classification is collected in Table 5. In Figure 5 we provide a synoptic view of all ETG nuclei in classes 3 and 4.

4.3 Individual notes about MIR classification

NGC 4261 (E3) The galaxy (see Figure 4) is borderline between class-4 and class-2. The galaxy displays a MIR spectrum similar to that of NGC 4486 (see Figure 5). At odds with NGC 4486, the spectrum of this galaxy shows the high ionization [NeV] 14.32 μm emission line and likely a dusty torus is needed to fully account for the observed continuum, in addition to a synchrotron component.

NGC 4383 (S0:) This galaxy was included in MIR class-3 because of its PAH inter-band ratio $(\mathrm{PAH}_{7.7\mu m}/\mathrm{PAH}_{11.3\mu m} = 4.6)$. However, it presents the steepest and strongest MIR continuum of any ETG in class-3. The analysis of the spectrum shows that the slope of the MIR continuum, calculated as $\mathrm{F}_\nu(30\mu m)/\mathrm{F}_\nu(15\mu m) = 6.7$, is consistent with the values found in starburst galaxies (see e.g. Brandl et al. 2006). Furthermore, the [NeIII] 15.5 μm /[NeII] 12.8 μm vs. [SIII] 33.5 μm/ [SiII] 34.8 μm diagnostic diagram (see Dale et al. 2006) locates the galaxy in the starburst region. All of these indicate that the class-3 classification points to the presence of on-going star formation in the nucleus.

The lower values of the MIR slopes shown by the remaining class-3 objects in Figure 5 (2.3 for NGC 3258, 1.2 for NGC 3268, 4.2 for NGC 5018 and 4.5 for NGC 4435 (Panuzzo et al. 2007)) may indicate that the starburst phase in these objects is fading and there are not as many ionizing stars to heat the dust as in the peak of the starburst phase.
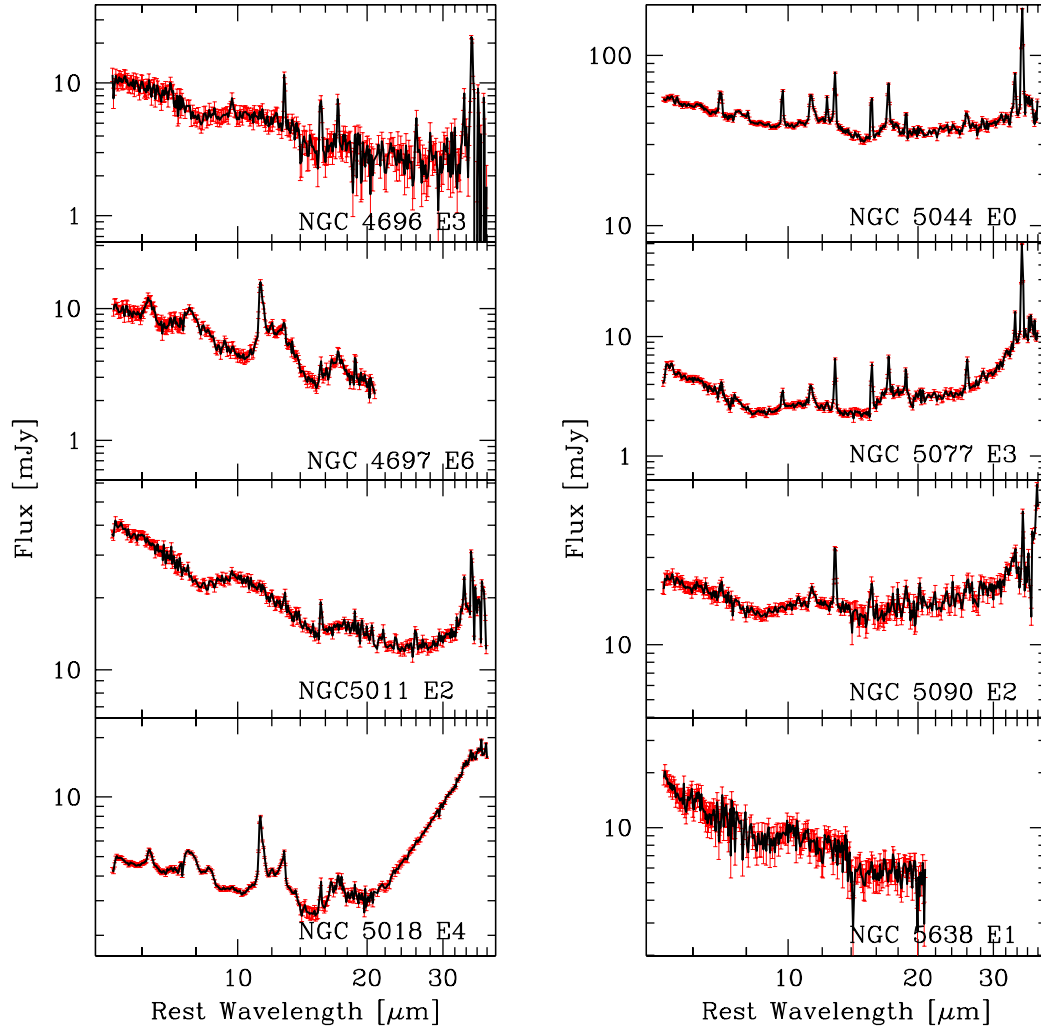
Figure 1. *(cont.)* MIR spectra of Es.

This has been discussed in some detail by Panuzzo et al. (2007) for the case of NGC 4435.

NGC 5128 Cen A (S0+S pec)   The most striking feature in its IRS spectrum is the strong silicate absorption feature at 9.7 μm. This feature is weak or seen in emission in the other class-4 galaxies of the sample. Sargsyan et al. (2011) found this feature typical of the so called "absorption AGN" while "emission AGN" have spectra similar to our MIR class-4 spectra. Such a strong absorption is an indication of an enormous amount of extinction towards the nucleus, which is probably embedded in a very dusty and compact torus (see e.g. Armus et al. 2007).

NGC 5273(S0/a)   The galaxy was included in class-4 because of its large MIR excess over the underlying stellar population continuum. Unfortunately the spectrum does not include the SL2 module (see Table 4).

5   DEMOGRAPHY OF MIR SPECTRAL PROPERTIES OF ETGS

In the following sub-sections we investigate the MIR spectra and their classes as a function of the properties of the host galaxy in a multi-wavelength context. Adopting a Poisson statistics, for each percentage we obtained single-sided upper and lower limits, corresponding to 1σ Gaussian errors (Gehrels 1986).

5.1   MIR classes vs. morphological classification and galaxy environment

We summarize the data concerning MIR classes versus E and S0 morphological classes and the galaxy environment in Table 6.

Es are significantly more passive than S0s: $46^{+11}_{-10}\%$ of Es and $20^{+11}_{-7}\%$ of S0s have a class-0 spectrum.

S0s show the tendency to be more gas rich than Es: $80^{+18}_{-15}\%$ of S0s and $54^{+11}_{-10}\%$ of Es belong to classes
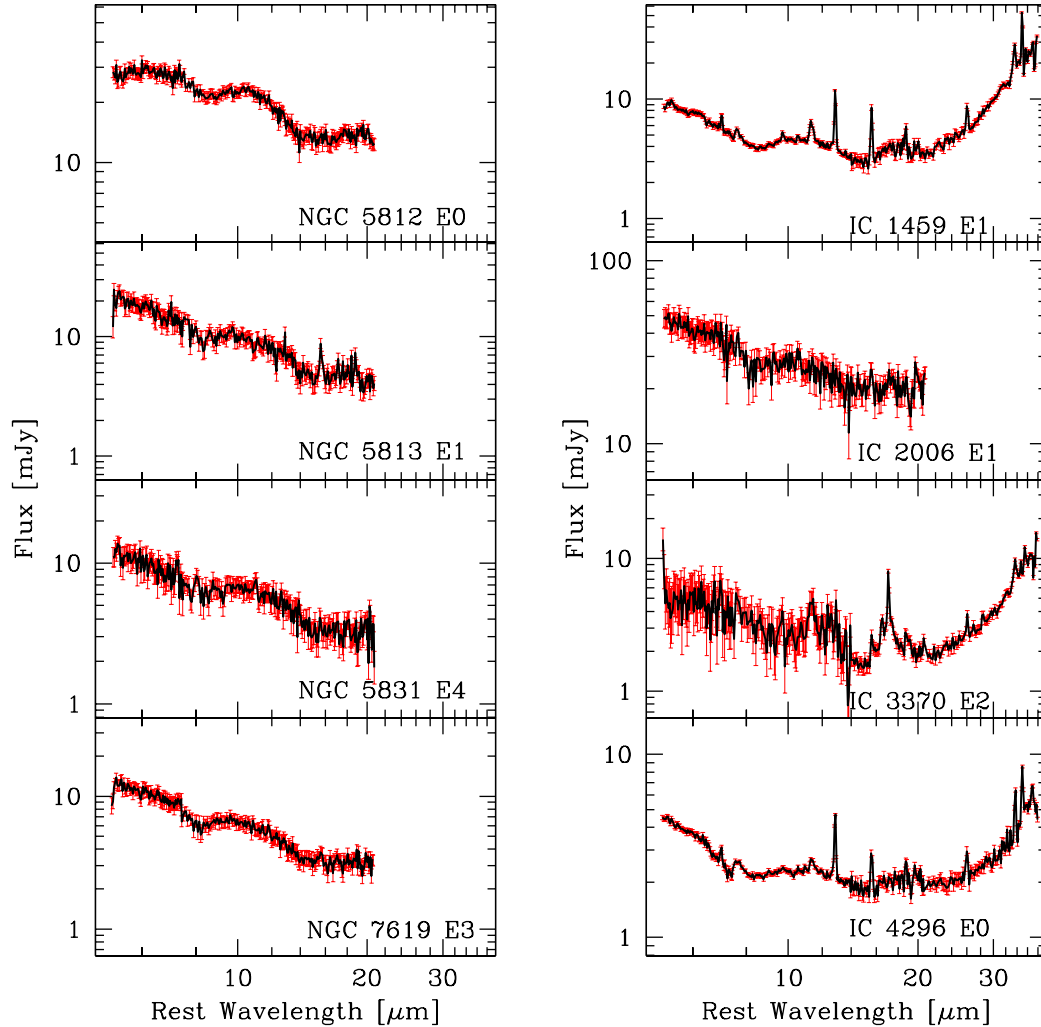
Figure 1. *(cont.)* MIR spectra of Es. For IC 3370 (see Kaneda et al. 2008), the SL observations miss the center of the galaxy by $10''$, which caused significant reduction in the S/N ratio of the SL spectrum.

1, 2, 3 and 4 showing emission lines. Considering the whole sample of ETGs, $64^{+12}_{-6}\%$ of the nuclei show emission lines, although with different intensity. This is in agreement with optical studies, in which, depending on the sample (sometimes strongly biased against passively evolving objects) the ionized gas is detected in ≈50-90% of ETGs (Phillips et al. 1986; Macchetto et al. 1996; Sarzi et al. 2006, 2010; Yan et al. 2006; Serra et al. 2008; Annibali et al. 2010).

$41^{+10}_{-9}\%$ of Es and $57^{+16}_{-13}\%$ of S0s show PAH emission, indicating that in about half ($47^{+8}_{-7}\%$) of ETGs a star formation episode has occurred about 10^8 years ago (Kaneda et al. 2008; Panuzzo et al. 2011). Galaxies with normal PAH ratios, class-3 spectra, are a minority both amongst Es and S0s: only $9^{+4}_{-3}\%$ show star forming spectra.

Panuzzo et al. (2011) considered the ratio between the class-2 and class-3 spectra in the hypothesis that anomalous PAHs in class-2 are produced by carbon stars (Vega et al.

2010). For solar metallicity, carbon stars are present in stellar populations with ages between $\sim$ 250 Myr and $\sim$ 1.3 Gyr (Marigo & Girardi 2007). Assuming a characteristic life-time of 200 Myr for a star formation episode (Panuzzo et al. 2007) the expected ratio between ETGs with $PAH_{anomalous}/PAH_{normal}$ is between 1 and 7. Here we obtain a ratio of 3.5, half of that reported in Panuzzo et al. (2011).

All MIR class-4 spectra show PAHs, suggesting that the AGN phenomenon is associated with star formation. Class-4 MIR spectra (Figure 5 bottom panel) include 3 E and 4 S0 galaxies, corresponding to $8^{+4}_{-3}\%$ of our ETG sample.

The fraction of Es with PAH features (classes 2, 3 and 4) in clusters tends to be lower than that in LDEs ($20^{+19}_{-11}\%$ vs. $49^{+13}_{-11}\%$), suggesting that star formation episodes are triggered in LDEs. The PAH features of S0s show a similar percentage in clusters and in LDEs ($44^{+23}_{-16}\%$ vs. $68^{+25}_{-19}\%$). These results are consistent with other indicators that find ETGs
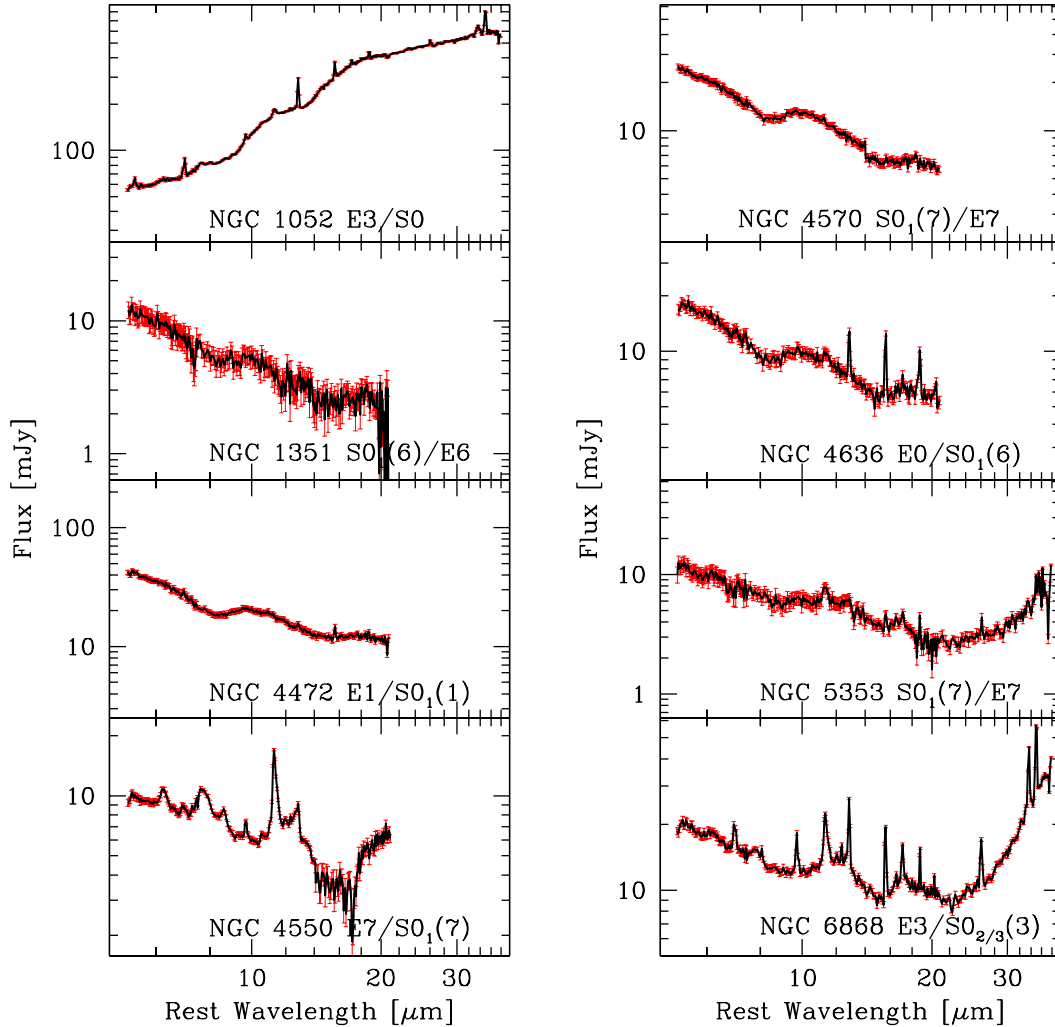
Figure 1. *(cont.)* MIR spectra of E/S0s. In the case of NGC 4472 the LL2 module has been arbitrarily scaled.

located in high density environments older (Clemens et al. 2006, 2009) and, in general, less "active" (Moore et al. 1996; Feldmann et al. 2011, to mention theoretical approaches) than their counterparts in groups and in the field.

5.2   MIR classes and the hot nuclear gas

In the top panel of Figure 6, we plot the nuclear X-ray luminosity, $L_{X,nuc}$ versus the MIR classes. The $L_{X,nuc}$ (Table B1, columns 4 and 9, Pellegrini 2010) refers to a central aperture ($\sim 2''$ radius) in the 2-10 keV bands of *Chandra* observations (Pellegrini, private communication). The $L_{X,nuc}$ aperture lies within the *Spitzer*-IRS slit width and allows us to investigate the presence of the AGN engine and the role of the X-ray radiation field on the MIR spectra.

ETGs in class-4 have the higher values of $L_{X,nuc}$, as expected from the presence of an AGN. The analysis of X-ray spectra in a sub-sample of our ETGs, obtained with *Chandra* and XMM-*Newton* data, show that a power law component

is needed to account for the observed emission of all ETGs in class-4 (González-Martìn et al. 2009; Boroson et al. 2011; Machacek et al. 2004; Capetti & Balmaverde 2006; Grützbauch et al. 2007; Ghosh et al. 2005).

ETGs in class-0 show low values of $L_{X,nuc}$ ($\sim 10^{38} - 10^{39}$ erg s^{-1}, see Figure 6), with some exceptions. The X-ray spectral analysis of the class-0 NGC 720, NGC 821, NGC 1399 need an AGN contribution at odds with NGC 1427, NGC 3379, NGC 3377, NGC 3608, NGC 4473. Pellegrini (2010) remarks indeed the large spread of $L_{X,nuc}$ and suggests that it could be produced by the nuclear activity cycle, where $L_{X,nuc}$ is regulated by the joint actions of the feedback and the fuel availability.

High values of $L_{X,nuc}$ are also found in ETGs of classes 1 and 2 and partly of class-3, likely reflecting the contribution of an AGN. In particular, an AGN contribution has been detected in the X-ray spectra of NGC 1404, NGC 4649 and NGC 5846 of class-1; NGC 1553, NGC 2685, NGC 4036, NGC 4374, NGC 4552, IC 1459, NGC 5090 of class-2; NGC
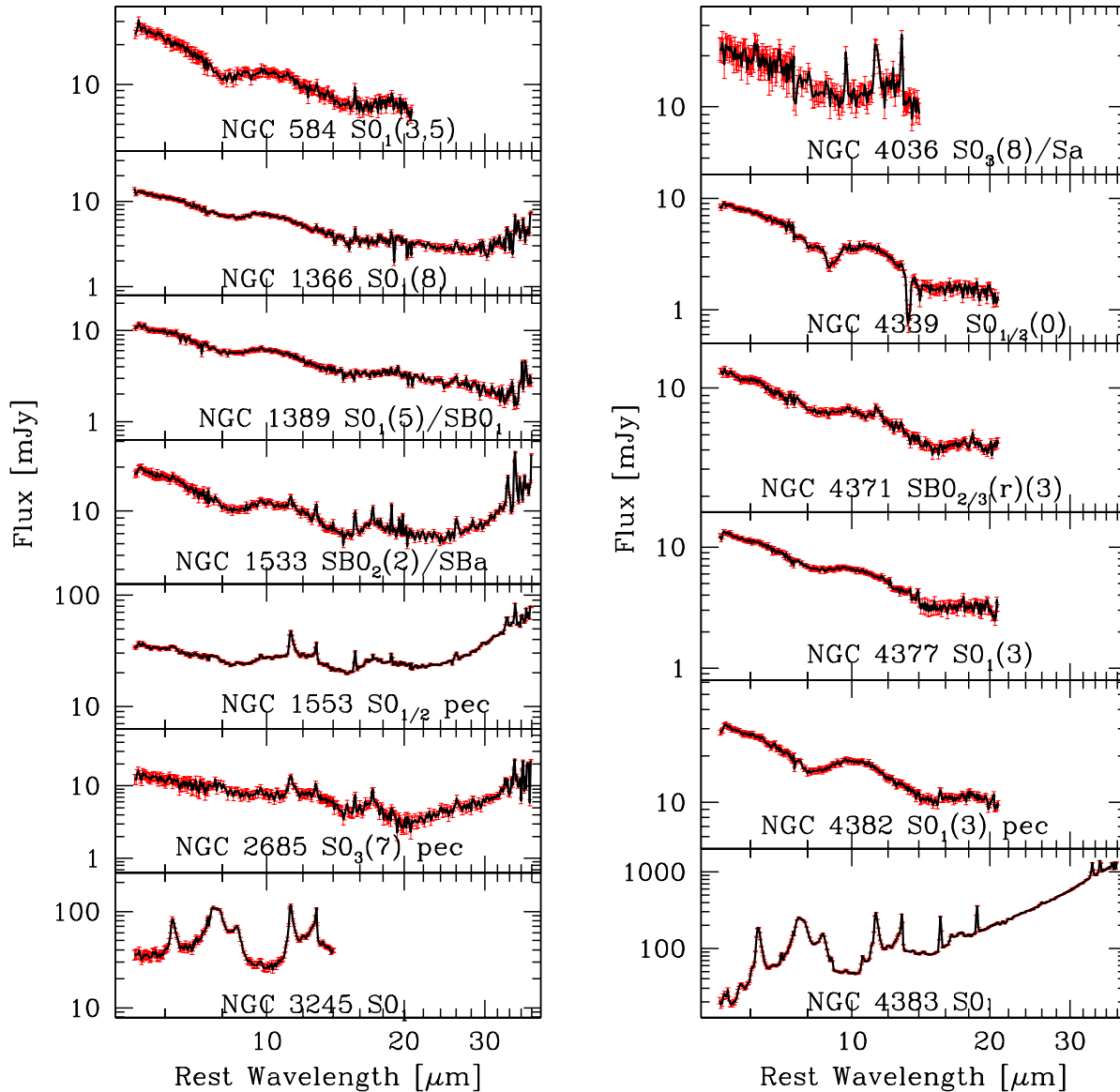
Figure 1. *(cont.)* MIR spectra of S0s and SB0s. The spectrum of NGC4339 shows absorption features at 9 and 13 μm which are data reduction artifacts due to a bright source falling in the peak-up blue FOV during the observation.

3245, NGC 4435, NGC 4697, NGC 5018 of class-3. No AGN contribution is required neither to model the X-ray spectra of NGC 584 (class-1) nor NGC 4589 and NGC 4696 (class-2).

X-ray cavities are considered signatures of the AGN feedback (Cavagnolo et al. 2010, and references therein). *Chandra* observations detected X-ray cavities in many of our ETGs (NGC 3608 in class-0; NGC 4472, NGC 4649, NGC 5813, NGC 5846 in class-1; NGC 1553, NGC 4552, NGC 4636, NGC 5044, IC 4296 in class-2; NGC 4261 in class-4) suggesting an evolutionary link between MIR classes.

5.2.1 $11.3\mu m/7.7\mu m$ PAH ratio and the hot nuclear gas

In the bottom panel of Figure 6, we plot the ratio between the PAH features at 11.3μm and 7.7μm versus $L_{X,nuc}$. Although the dispersion is quite large, the figure shows a weak relation (the Pearson correlation coefficient is $r = 0.58$) between the PAH 11.3/7.7 μm ratio and $L_{X,nuc}$. Draine & Li (2007) suggested that variations in PAH emission ratios can be accounted for by the combined effects of variations in exciting radiation, PAH size and ionization state. The nuclear X-ray radiation field seems indeed to play a role in the determination of the PAH 11.3/7.7 μm ratio, taking into account the large variation of $L_{X,nuc}$ reported by Pellegrini (2010). ETG nuclei in class-3 (normal PAH ratios), have a lower
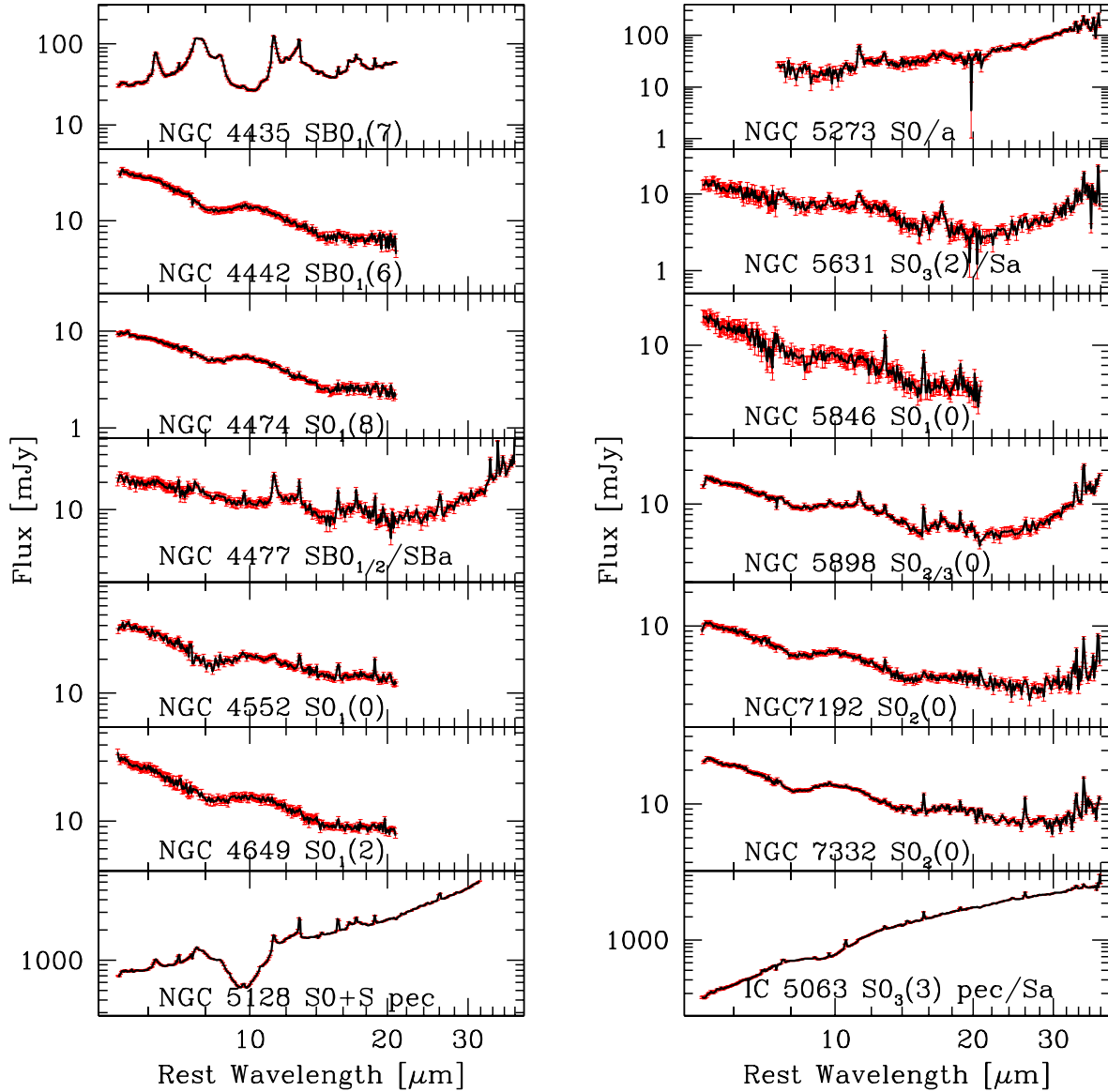
Figure 1. *(cont.)* MIR spectra of S0s and SB0s.

$L_{X,nuc}$ emission compared to ETGs with anomalous PAH ratios, as shown by the median values (large open squares in Figure 6 bottom panel) of classes 2 and 4.

5.3   MIR classes, MIR atomic line diagnostics and H_2 emission

We report in Table B1 (columns 3 and 8) the optical activity class of the ETG nuclei (Ho et al. 1997; Annibali et al. 2010). A large fraction of them are LINERs in the optical window since they show low ionization emission lines. Among optical LINERs, MIR classes well identify both passively evolving ETGs and star forming nuclei (Rampazzo et al. 2011, their Figure 2). However, what pow-

ers the remaining objects of the vast class of LINERs is still debated.

In Figure 7, MIR classes 1 to 4 are plotted in the Ne[III]15.5μm/[NeII]12.8μm vs. [SIII]33.5μm/[SiII]34.8μm plane (Dale et al. 2006). The plot indicates the areas in which AGN, LINERs and starburst (SB) galaxies are typically located. Similarly to optical diagnostic diagrams (e.g. Annibali et al. 2010) the MIR line diagnostic is unable to fully separate powering mechanisms. ETGs in class-3, but NGC 3258, inhabit the SB sector, mix together with class-2 galaxies, although the two classes have totally different PAH ratios i.e. different star forming properties. ETGs in class-2 mix also with class-4, suggesting the presence of an AGN contribution. The class-4 NGC 4261, a LINER in the
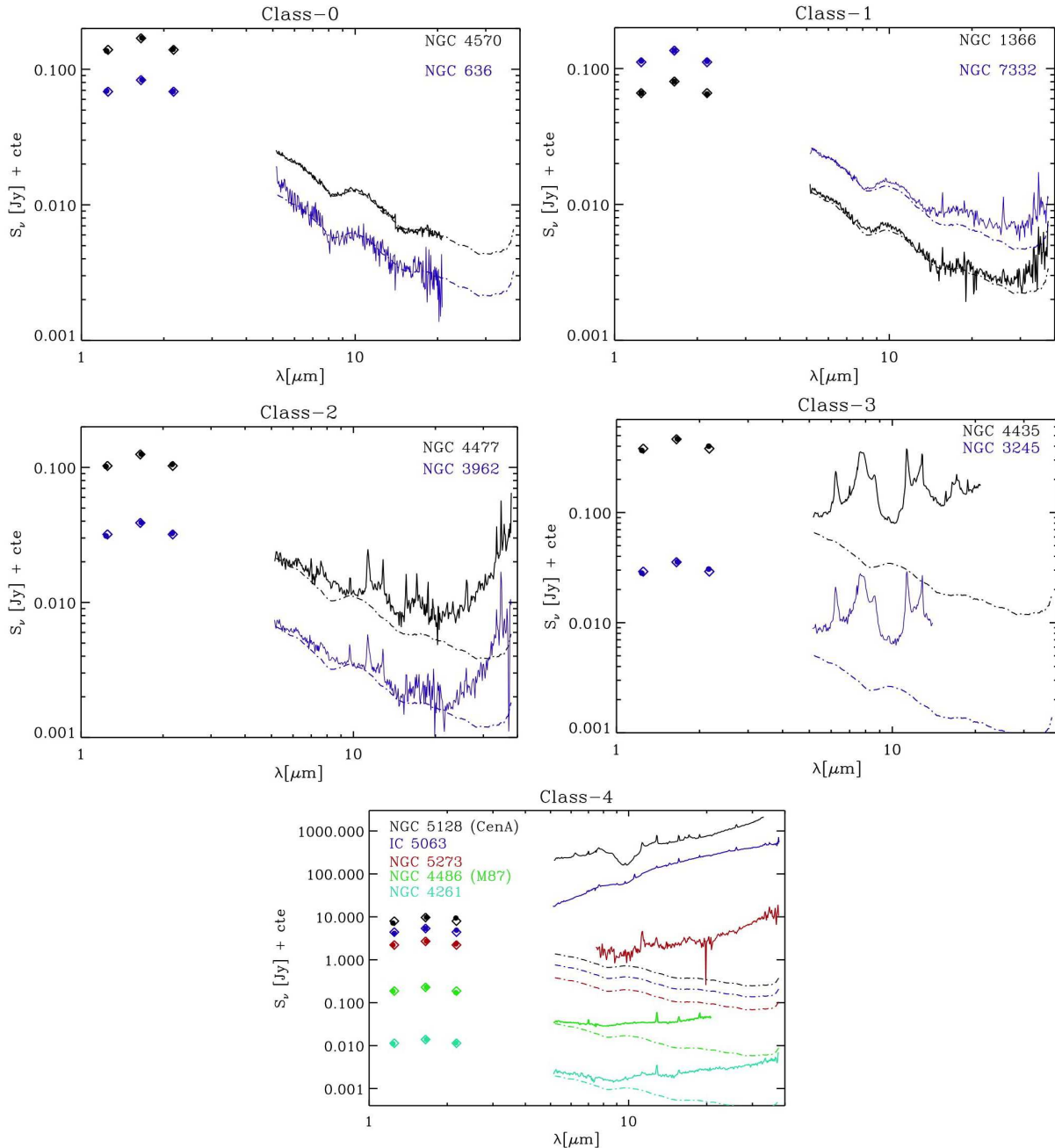
Figure 2. Comparison of the passive template used in this work (dotted-dashed line) and the MIR spectra (solid line) of different galaxies with different degrees of MIR activity. The template has been normalized to the H-band flux of each galaxy. The 2MASS J, H, K-band fluxes of the galaxies, within the central 5″ radius, are indicated with filled circles, while the corresponding normalized values of the template are plotted as open diamonds.

optical, is located in the SB region of Figure 7. In the MIR, its AGN nature is suggested by the presence of an excess over the passive stellar continuum, similarly to NGC 4486, and by the high ionization [NeV] 14.32 μm emission line, as well as, in X-rays, by the detection of a central AGN and cavities.

In the current literature, low accretion rate AGNs are the favoured mechanism for ionizing LINERs. Considering that massive black holes are thought to be present in galaxies with a spheroidal component (e.g. Kormendy et al. 2004), the above mechanism is supported by the pres-

ence of compact X-ray and/or nuclear radio sources (González-Martìn et al. 2009), UV and X-ray variability (Maoz et al. 2005; Pian et al. 2010) and broad emission lines in the optical spectra. However, there is evidence for a deficit of ionizing photons from weak AGN suggesting that more than one excitation mechanism may operate in LINERs (see Eracleous et al. 2010). Also the photoionization by old post-asymptotic giant branch (post-AGB) stars (Trinchieri et al. 1991; Binette et al. 1994; Stasińska et al. 2008) can account for the ionizing photon budget only in the weakest LINERs, or in off-nuclear regions (Annibali et al. 2010).
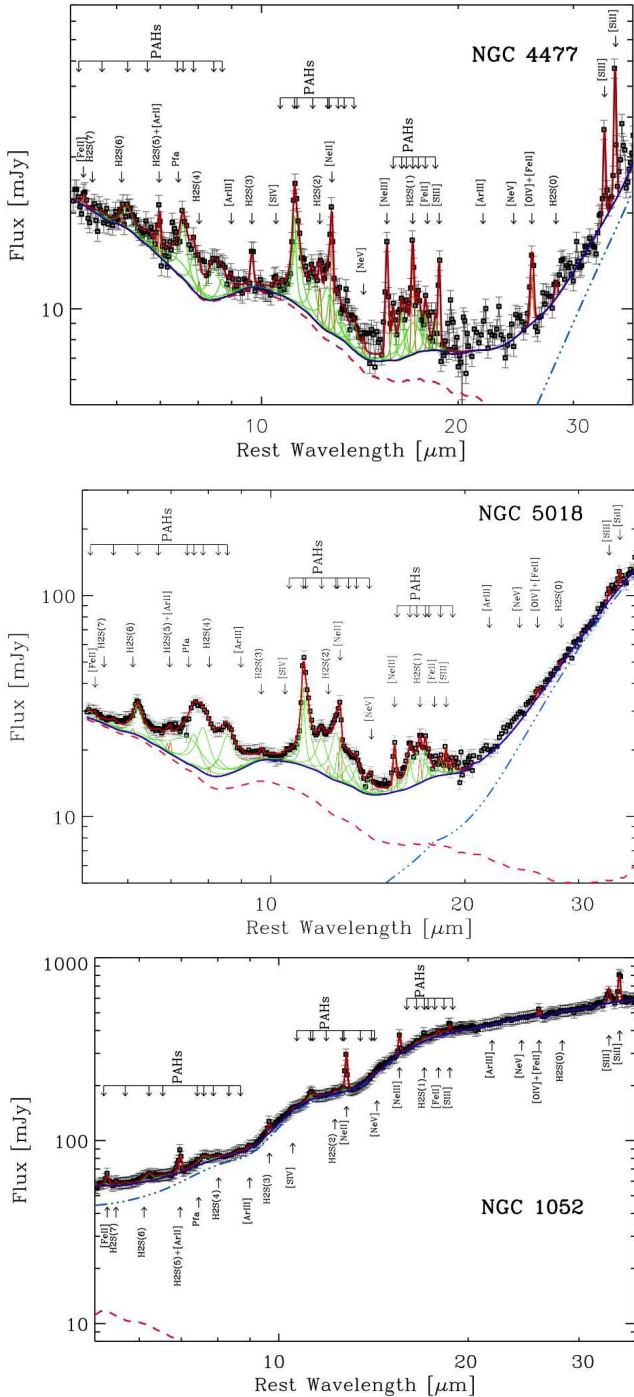
Figure 3. Best fit of the spectrum of three ETGs with anomalous PAH emissions (upper panel), normal PAH emissions (middle panel), and steep MIR continuum (bottom panel). Open squares and the solid thick red line are the observed MIR spectra and our final best fit, respectively. The fit is calculated as the sum of an underlying continuum (solid thick blue line), the PAH features (solid thin green line) and the emission lines (solid thin orange line). The two components of the continuum, old stellar population (dashed red line) and diffuse dust emission (dot-dashed blue line), are also plotted.

For a long time, shocks (Koski et al. 1976; Heckman 1980; Dopita et al. 1995; Allen et al. 2008) have been proposed as a possible gas ionization mechanism in ETG nuclei. The shock scenario may be related to the presence of the H_2 molecular emission that is thought to be an important coolant in post-shock regions (Roussel et al. 2007; Ogle et al. 2007). We found $H_2S(1)$ line with similar rates in Es ($34^{+10}_{-8}\%$) and S0s ($51^{+15}_{-12}\%$). Several galaxies with X-ray cavities indeed show H_2 emission, like NGC 1553, NGC 4374, NGC 4552, NGC 4636, NGC 5044, NGC 5813 and IC 4296, as well as MIR class-4 galaxies with X-ray detected AGN, like NGC 1275, NGC 1052, NGC 4036 and NGC 5128. However, the largest fraction of H_2 emitters is found among MIR class-2 galaxies.

5.4 MIR classes and CO

In this section we report about CO observations, with the aim of investigating MIR classes vs. ETGs cold gas content.

41 galaxies of our sample are included in the survey of 260 ETGs in ATLAS^{3D} (Young et al. 2011). Only 6 out of 41 ($15^{+9}_{-6}\%$) were detected: 4 (NGC 4036, NGC 4435, NGC 4477, NGC 5273) in both in CO ($J = 1 - 0$) and ($J = 2 - 1$) and 2 (NGC 2685 and NGC 3245) in the ($J = 1 - 0$) line. Detected galaxies are S0s and none belong to MIR classes 0 or 1. NGC 2685, NGC 4036 and NGC 4477 are of MIR class-2; NGC 3245, NGC 4435 of class-3 and NGC 5273 of class-4. Their molecular gas masses are in the range $7.27 <$ log $M(H_2) < 8.13$ $M_\odot$ (Young et al. 2011).

NGC 4550 and NGC 4697 of class-3 are undetected in Young et al. (2011). Wiklind & Henkel (2001) and Sofue & Wakamatsu (1993) detected NGC 4550 and NGC 4697 (together with class-2 NGC 4589), respectively, in the CO ($J = 1 - 0$) line. In this line, it is also detected the class-3 S0 NGC 4383 (Thronson et al. 1989).

NGC 4261 and NGC 4486, in class-4, were undetected by Young et al. (2011) (see also Ocaña Flaquer et al. (2010) for NGC 4261). Smolcić & Riechers (2011) detected NGC 4486 in the ($J = 1 - 0$) line. Several ETGs of class-4 have been detected in CO, namely NGC 1052 (Welch et al. 2010, ($J = 2 - 1$)), NGC 1275 (Salomé et al. 2006) and NGC 5128 (Morganti 2010) and IC 5063 (Morganti et al. 2013, in CO ($J = 2 - 1$)). Their H_2 masses differ by orders of magnitude scaling down from about 10^{10} $M_\odot$ in NGC 1275, to 10^8 $M_\odot$ in NGC 5128 and in IC 5063 and to about 10^7 $M_\odot$ in NGC 1052.

Summarizing, all ETGs detected in CO lines show PAHs, either with normal or anomalous ratios, in their MIR nuclear spectra.

5.5 MIR classes and the radio continuum at 1.4 GHz

A large fraction of ETGs in the present sample are radio emitters, although with different radio intensities, morphologies and classes. In Table B1 (columns 5 and 10) we report the 1.4 GHz radio power catalogued by Brown et al. (2011). These authors found that the radio powers of ETGs, with similar M_K magnitude, may vary by roughly than two orders of magnitude over long periods of time. The radio power may keep trace of the past activity (AGN and/or star for-
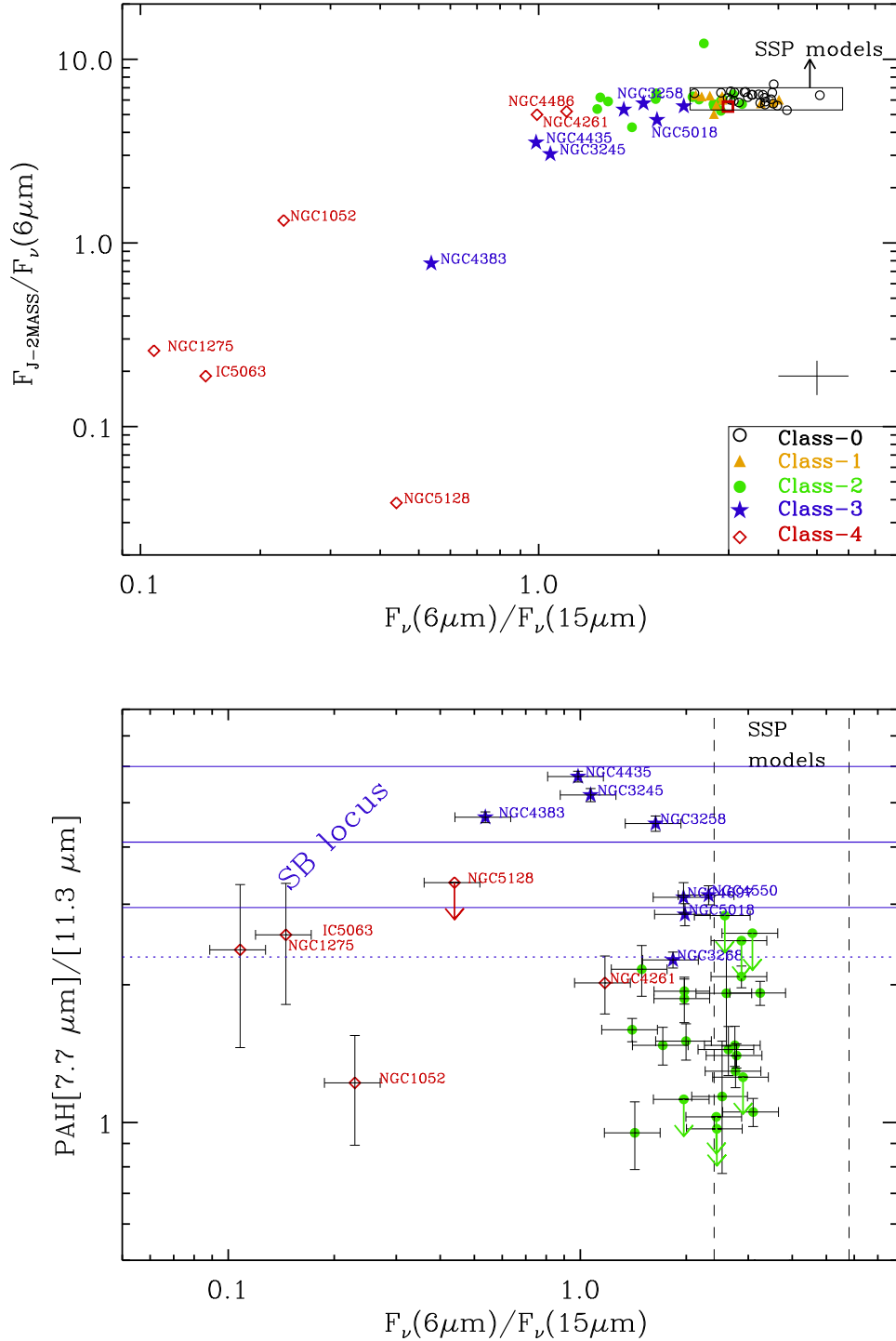
Figure 4. (*Top panel*) Color-color plot of the 2MASS J-band/6μm vs. the 6μm/15μm flux ratios. The rectangle encloses Single Stellar Population (SSP) models of ETGs with ages in the interval 10–14.5 Gyr and metallicty, Z, in the range 0.004–0.05. The red open square within the rectangle represents a 12 Gyr old SSP model with solar metallicity. The typical error is also shown. (*Bottom panel*) The 7.7μm/11.3μm PAH ratio vs. the 6μm/15μm flux ratio. The dotted horizontal line correspond to cirrus emission (Lu et al. 2003). Solid horizontal lines mark the region of the HII dominated sources or starburst galaxies (SB), the central line is the median 4.2 value (Smith et al. 2007). The dashed vertical lines mark the area of old SSP models described above.
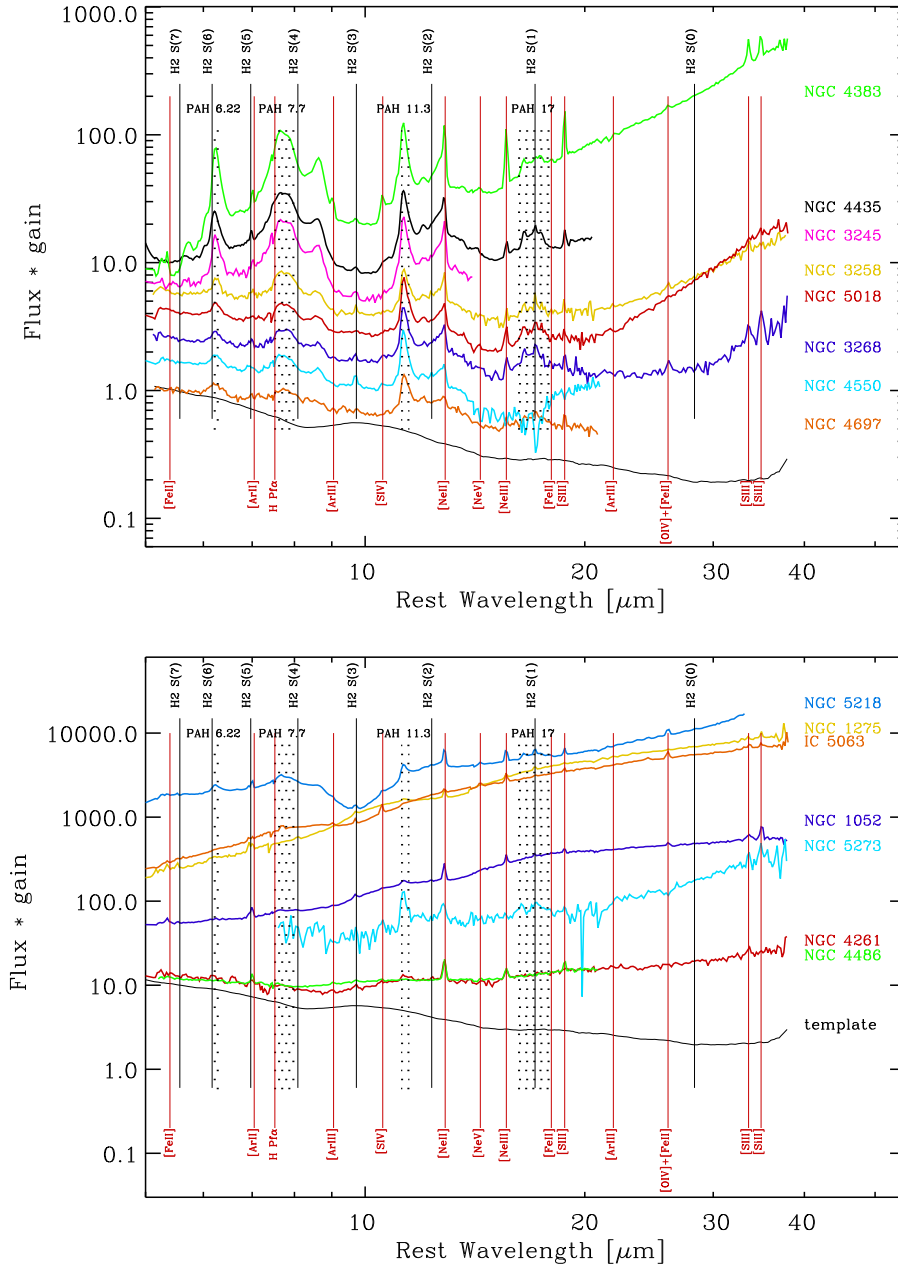
Figure 5. Examples of ETGs with MIR class-3 (top panel) and class-4 (bottom panel) spectra. Fluxes have been normalized to the template and then arbitrarily scaled. PAH features (dotted area) typical of star forming galaxies together with ionic and/or molecular H_2 emission lines (solid lines), are detected in these spectra. The template passive spectrum is also shown.

mation) useful to investigate the possible link between MIR classes.

Figure 8 (top left panel) shows the distribution of the 1.4 GHz radio power vs. M_K magnitude. All ETGs brighter than -25.2 mag. are detected. According to Brown et al. (2011), massive galaxies always host an AGN or have recently undergone star formation. The top right panel of Figure 8 shows M_K magnitude vs. MIR classes. Each MIR class covers roughly the full range of M_K.

The $P_{1.4GHz}$ vs. MIR class suggests the following considerations. Although with a large dispersion, the class-4 includes the more powerful radio sources (Figure 8, bottom panel) . Star forming, class-3, ETGs have intermediate/low radio power. A star formation rate of ~ 1 $M_\odot$ yr^{-1} is expected to produce 10^{21} W Hz^{-1} of radio emission in ETGs (Wrobel & Heeschen 1988; Bell 2003). The Milky Way (indicated in the plot) has a radio power $P_{1.4GHz} \simeq 4 \times 10^{21}$ W Hz^{-1}. In class-2, the stronger radio emitters are ETGs with X-ray cavities, likely connected to the AGN feedback (Cavagnolo et al. 2010). X-ray cavities are also detected in class-1 and in the E of class-0 NGC 3608 (M_K=-24.80), detected at 1.4 GHz.

ETGs in class-0 set the lower boundary of the $P_{1.4GHz}$ radio power. Remarkable exceptions are NGC 1407 and
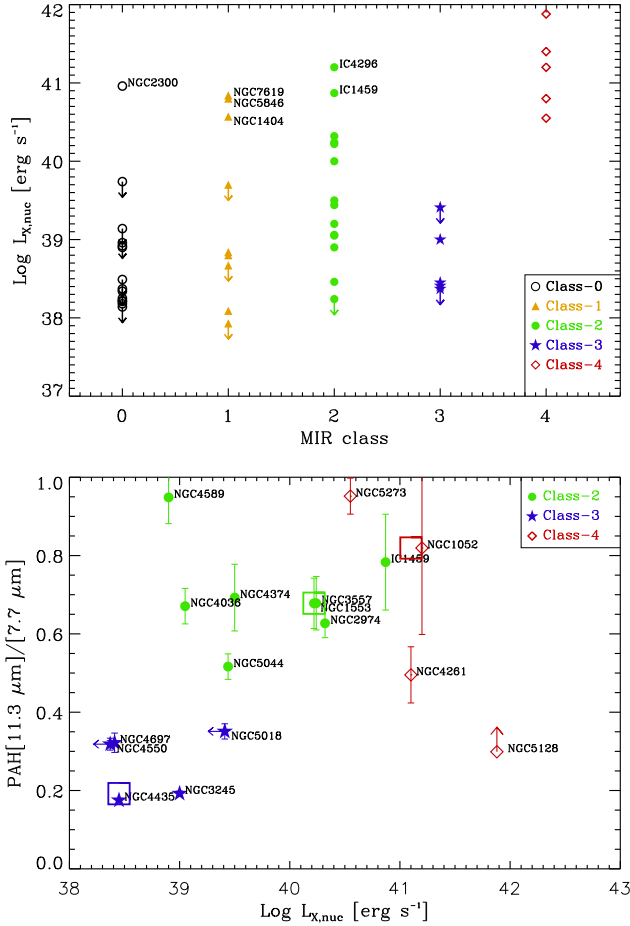
Figure 6. (*Top panel*) Galaxy nuclear X-ray luminosity, Log $L_{X,nuc}$, (Pellegrini 2010) vs. MIR classes. X-ray bright galaxies of classes 0, 1, 2 are labeled. (*Bottom panel*) The ratio of PAH features at 11.3 and 7.7 μm vs. Log $L_{X,nuc}$. Arrows represent upper limits and are colour coded as the detections. The large, open squares represent the median value of detected objects in each class. The bottom right diamond refers to the PAH ratio measured for NGC 5128. The strong absorption centred at 10μm (see Figure 1) probably perturbs the measure of the PAH line strength so that the PAH ratio is likely a lower limit. Therefore, in addition to the diamond, we label it with an arrow.

NGC 1399. These are among the brightest ($M_K \leqslant -25.3$) Es in the sample, have radio jets (Van Velzen et al. 2012) and X-rays detected AGN in their nuclei (Pellegrini 2005). A misalignment of the SL and LL slits with respect to the jet position angle may explain the class-0 spectrum of these galaxies. In the case of NGC 4486, the jet is sampled only by the LL slits, notwithstanding Buson et al. (2009) detected the synchrotron emission.

6 MIR CLASSES AND ACCRETION SIGNATURES

Panuzzo et al. (2011) suggested that an accretion event may cause a passively evolving ETG (class-0) to ignite star formation (class-3) and/or feeding the central black hole, revitalizing the AGN activity (class-4). We review here possible

Table 5. MIR spectral classes

Ident.	Morpho. RSA	MIR class	Ident.	Morpho. RSA	MIR class
NGC 636	E1	0	NGC 5090	E2	2
NGC 720	E5	0	NGC 5638	E1	0
NGC 821	E6	0	NGC 5812	E0	0
NGC 1209	E6	1	NGC 5813	E1	1
NGC 1275	E pec	4	NGC 5831	E4	0
NGC 1297	E2	2	NGC 7619	E3	1
NGC 1339	E4	0	IC 1459	E1	2
NGC 1374	E0	0	IC 2006	E1	1
NGC 1379	E0	0	IC 3370	E2 pec	2
NGC 1395	E2	2	IC 4296	E0	2
NGC 1399	E1	0			
NGC 1404	E2	1	NGC 1052	E3/S0	4
NGC 1407	E0	0	NGC 1351	S0$_1$/E6	0
NGC 1426	E4	0	NGC 4472	E1/S0$_1$	1
NGC 1427	E5	0	NGC 4550	E/S0	3
NGC 1453	E2	2	NGC 4570	E7/S0$_1$	0
NGC 1549	E2	2	NGC 4636	E0/S0$_1$	2
NGC 1700	E3	1	NGC 5353	S0$_1$/E7	2
NGC 2300	E3	0	NGC 6868	E3/S0$_{2/3}$	2
NGC 2974	E4	2	NGC 584	S0$_1$	1
NGC 3193	E2	0	NGC 1366	S0$_1$	1
NGC 3258	E1	3	NGC 1389	S0$_1$/SB0$_1$	0
NGC 3268	E2	3	NGC 1533	SB0$_2$/SBa	2
NGC 3377	E6	0	NGC 1553	S0$_{1/2}$ pec	2
NGC 3379	E0	0	NGC 2685	S0$_3$ pec	2
NGC 3557	E3	2	NGC 3245	S0$_1$	3
NGC 3608	E1	0	NGC 4036	S0$_3$/Sa	2
NGC 3818	E5	0	NGC 4339	S0$_{1/2}$	0
NGC 3904	E2	0	NGC 4371	SB0$_{2/3}$(r)	2
NGC 3962	E1	2	NGC 4377	S0$_1$	0
NGC 4261	E3	4	NGC 4382	S0$_1$ pec	1
NGC 4365	E3	0	NGC 4383	S0:	3
NGC 4374	E1	2	NGC 4435	SB0$_1$	3
NGC 4473	E5	0	NGC 4442	SB0$_1$	0
NGC 4478	E2	0	NGC 4474	S0$_1$	0
NGC 4486	E0	4	NGC 4477	SB0$_{1/2}$/SBa	2
NGC 4564	E6	0	NGC 4552	S0$_1$	2
NGC 4589	E2	2	NGC 4649	S0$_1$	1
NGC 4621	E5	0	NGC 5128	S0+S pec	4
NGC 4660	E5	0	NGC 5273	S0/a	4
NGC 4696	E3	2	NGC 5631	S0$_3$/Sa	2
NGC 4697	E6	3	NGC 5846	S0$_1$	1
NGC 5011	E2	1	NGC 5898	S0$_{2/3}$	2
NGC 5018	E4	3	NGC 7192	S0$_2$	1
NGC 5044	E0	2	NGC 7332	S0$_{2/3}$	1
NGC 5077	E3	2	IC 5063	S0$_3$/Sa	4

accretion signatures, such as peculiarities in the morphology and kinematics of the galaxy and of the dust-lane structure.

6.1 Morphological and kinematical peculiarities

In Table B2 and Table B3 we collect the kinematical (column 3) and morphological (column 4) peculiarities described in the literature for Es and S0s, respectively. The kinematical notes consider the detection of counter rotation (CR), gas vs. gas, stars vs. gas and stars vs. stars, and of multiple kinematical components (MC), widely believed to be associated with accretion events (see e.g. Corsini et al. 1998; Krajnović et al. 2008;

Table 6. Demography of MIR spectral classes

MIR classes	E galaxies					S0 galaxies				
	0	1	2	3	4	0	1	2	3	4
Total Nr. of gal.	26	7	16	4	3	7	8	12	4	4
Nr. of gal. in cluster	10	2	1	0	2	6	3	4	3	0
Nr. of gal. in LDE	16	5	15	4	1	1	5	8	1	4

Notes: see text and Tables 1 and 2 for galaxy members of cluster or located in LDE.

Bois et al. 2012). Other kinematical peculiarities are reported, like rotation along the minor axis, a phenomenon often associated with galaxy triaxiality (Bertola et al. 1988). The morphological peculiarities include the detection of shells, tidal tails, peculiar isophote shapes that are believed to be associated with interaction and/or minor/major merger events (Thomson & Wright 1990; Thomson 1991; Dupraz & Combes 1986; Henquist & Quinn 1987a,b).

$41^{+8}_{-7}\%$ of ETGs show some form of kinematical peculiarity. The percentage is likely a lower limit since some galaxies do not have detailed kinematical studies. Many galaxies also show morphological peculiarities. The above rate is consistent with the findings ($53^{+10}_{-4}\%$) of van Dokkum (2005) obtained from the analysis of morphological peculiarities in a comparable sample of nearby ETGs. He concludes that the majority of today's most luminous Es in the field were assembled through mergers of gas poor, bulge dominated systems. However, the high fraction of ETGs nuclei with line emission we found ($64^{12}_6\%$) argues that the above "dry merger" scenario is not so relevant.

Although the column 4 in the Tables B2 and B3 is largely incomplete, due to a still limited number of 2D kinematical studies, it is evident that kinematical (and morphological) signatures of accretions are found also in passively evolving Es and S0s (e.g. NGC 3377, NGC 3608, NGC 4570, NGC 4621, NGC 4660, NGC 5831). The fact that ETGs in class-0 show kinematical/morphological peculiarities suggest these are long lasting structures with respect to spectroscopic features: galaxies were active in the recent past, as traced by the peculiar kinematics/structures, but their spectra have already evolved into a passive phase (see e.g. Longhetti et al. 2000, for shell galaxies). Another possibility is a "dry" (van Dokkum 2005) and *sterile* accretion, i.e. it did not induce a star formation/AGN episode. Despite the presence of kinematical/morphological distortions, the spectrum remains passive, as in the case of an unperturbed/quiescent galaxy.

6.2　Dust-lane peculiarities

In column 5 of Tables B2 and B3 a description of the observed dust-lanes in the nuclear region is provided. The dust-lane morphology is available for 48/56 Es and for 25/35 S0s. $50^{+12}_{-11}\%$ of Es and $32^{+16}_{-11}\%$ S0s do not show dust-lanes.

Dust in ETGs, including the most passive objects, is normally produced by the collective outflow of dusty gas from evolving AGB stars. The silicate emission from this dust explains the 10 μm feature seen in MIR ETGs spectra (Knapp et al. 1989; Athey et al. 2002).

However, the short lifetime of dust in the ETGs environment means that little dust can accumulate unless somehow shielded from the hot gas (Clemens et al. 2010). In addition, the distribution of this dust follows that of stars, so dust-lanes cannot be produced in this way.

The presence of dust-lanes and their asymmetries therefore points to an external origin for the dust. An external origin is also consistent with (1) the lack of any strong correlation between FIR and optical galactic luminosities (e.g. Forbes 1991; Goudfrooij & de Jong 1995; Trinchieri & Goudfrooij 2002); (2) warm, counter-rotating gas observed in some ETGs (see Tables B1 and B2), (3) the distorted morphology of the dust (e.g. Finkelman et al. 2012).

In $42^{+18}_{-13}\%$ of Es and $24^{+14}_{-9}\%$ of S0s the dust-lane morphology is irregular or chaotic. Dust-lanes are often associated with morphological and/or kinematic peculiarities. Irregular/chaotic dust-lanes are found in all MIR classes. Dust-lanes, some quite complex, are found in class-4 (NGC 1052, NGC 1275, NGC 5128, NGC 5273 and IC 5063). Some Es, like NGC 1407, NGC 4621, NGC 4660 and NGC 5831, with MIR class-0 spectra, do not have dust-lanes detected in the optical but display kinematical peculiarities, such as counter rotation or rotation along the apparent minor axis, suggesting that either dry accretion events or dust evaporation may have occurred.

7　SUMMARY AND CONCLUSIONS

We present homogeneously reduced and calibrated low resolution, *Spitzer*-IRS spectra of a sample of 91 ETGs ($T < 0$) in the *Revised Shapely Ames Catalog* (Sandage & Tammann 1987). We aim to provide a MIR atlas of well studied, nearby ETGs in the range $\sim 5 - 40$ μm.

The atlas provides a measure of the atomic and molecular emission lines and PAH intensities. We classify each spectrum into one of the 5 MIR spectral classes devised by Panuzzo et al. (2011) for characterizing passive (class-0) intermediate (class-1 and class-2), star forming (class-3) and AGN (class-4) nuclei. The main results are the following.

• The nucleus of $\approx 1/3$ ($36^{+7}_{-6}\%$) of nearby ETGs in the atlas has a MIR class-0 spectrum, i.e. passively evolving according to Bressan et al. (2006). Class-0 spectra are more frequently detected among Es than S0s ($46^{+11}_{-10}\%$ vs. $20^{+11}_{-7}\%$). ETGs in class-0 set the lower boundary of the $P_{1.4GHz}$ radio power, i.e. they are the most quiescent nuclei, on average. Relevant exceptions are the massive ($M_K <$ -25.2), class-0 Es in Fornax NGC 1399 and NGC 1407, both having a high $P_{1.4GHz}$ and a radio-jet.

About $78^{+22}_{-18}\%$ of Es and all S0s in class-0 show no dust-lanes in the optical, although some galaxies show kinematical and morphological distortion, pointing to the occurrence of a past accretion episode. Thus, class-0 ETGs include either genuinely unperturbed, passively evolving galaxies or systems in which the effect of accretion has already quenched.

• Emission lines are detected in $64^{+12}_{-6}\%$ of nuclei. The detection of emission lines in many galaxies that show kinematical evidence of merger events argues against the so-called
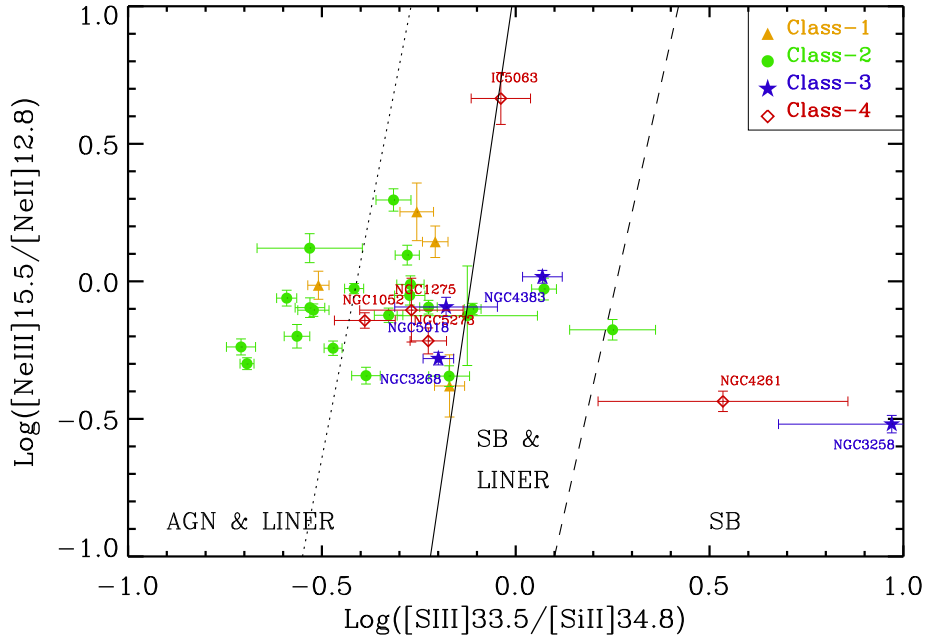
Figure 7. Emission line diagnostic diagram (from Dale et al. 2006) separating AGN from LINERs and star burst (SB) ETGs. We indicate MIR classes and have labeled some relevant galaxies.

"dry mergers" being an important formation mechanism for ETGs. H_2 molecular lines are also frequently detected: the $H_2S(1)$ emission line is detected in $34^{+10}_{-8}\%$ of Es and $51^{+15}_{-12}\%$ of S0s. PAH features (classes 2, 3 and 4), detected in $47^{+8}_{-7}\%$ of ETGs, tend to be less frequently found in cluster Es than in their LDE counterparts, suggesting a triggering of the star formation activity in LDEs. ETGs detected in the CO $(J = 1 - 0)$ and/or $(J = 2 - 1)$ lines show PAH complexes, either with normal or anomalous ratios, in their MIR nuclear spectra.

• A small fraction $(9^{+4}_{-3}\%)$ of ETGs shows class-3 spectra with normal PAH ratios, typical of star forming galaxies. The ratio between ETGs with normal (class-3) vs. anomalous (class-2) PAHs is consistent with being produced by a star formation episode with typical lifetime of 200 Myr. Class-3 ETGs have radio powers typical of star forming galaxies (Brown et al. 2011).

• The 11.3/7.7 μm PAH ratio weakly correlates with the galaxy X-ray nuclear luminosity, $L_{X,nuc}$, suggesting a dependence on the radiation field. Class-3 nuclei tend to be less luminous in X-rays with respect to both class-4 and class-2, where an AGN contribution may be present.

Panuzzo et al. (2011) suggest that each of the five MIR classes is a snapshot of the evolution of ETG nuclei during an accretion episode, starting from, and ending with, a class-0 spectrum. The MIR emission line diagnostic diagram (Dale et al. 2006) is unable to distinguish between the different powering mechanisms ionizing the ISM. MIR classes are successful in identifying those LINER nuclei powered by star formation (class-3). Most ETGs in class-4 indicate the presence of an AGN. Several mechanisms ionizing the ISM seem to be at work, especially in transition class 2 where (low accretion rate) AGN, shock fronts (X-ray cavities, H_2) and/or past star formation (PAHs) signatures combine. ETGs in class-1 may still show signatures of past activity like strong radio emission and X-ray cavities in some galaxies. The MIR class-1 continuum is indistinguishable from that of class-0, suggesting that this class marks the end of the active phase in the nucleus. Kinematical and/or morphological scars of recent accretion episodes are found in a large fraction $(41^{+8}_{-7}\%)$ of our ETGs, even in passively evolving galaxies, further supporting the view of an evolutionary link between the MIR classes and accretion/feedback phenomena.

REFERENCES

Allen, M. G., Groves, B. A., Dopita, M. A., Sutherland, R. S., Kewley, L. J. 2008, ApJS, 178, 20
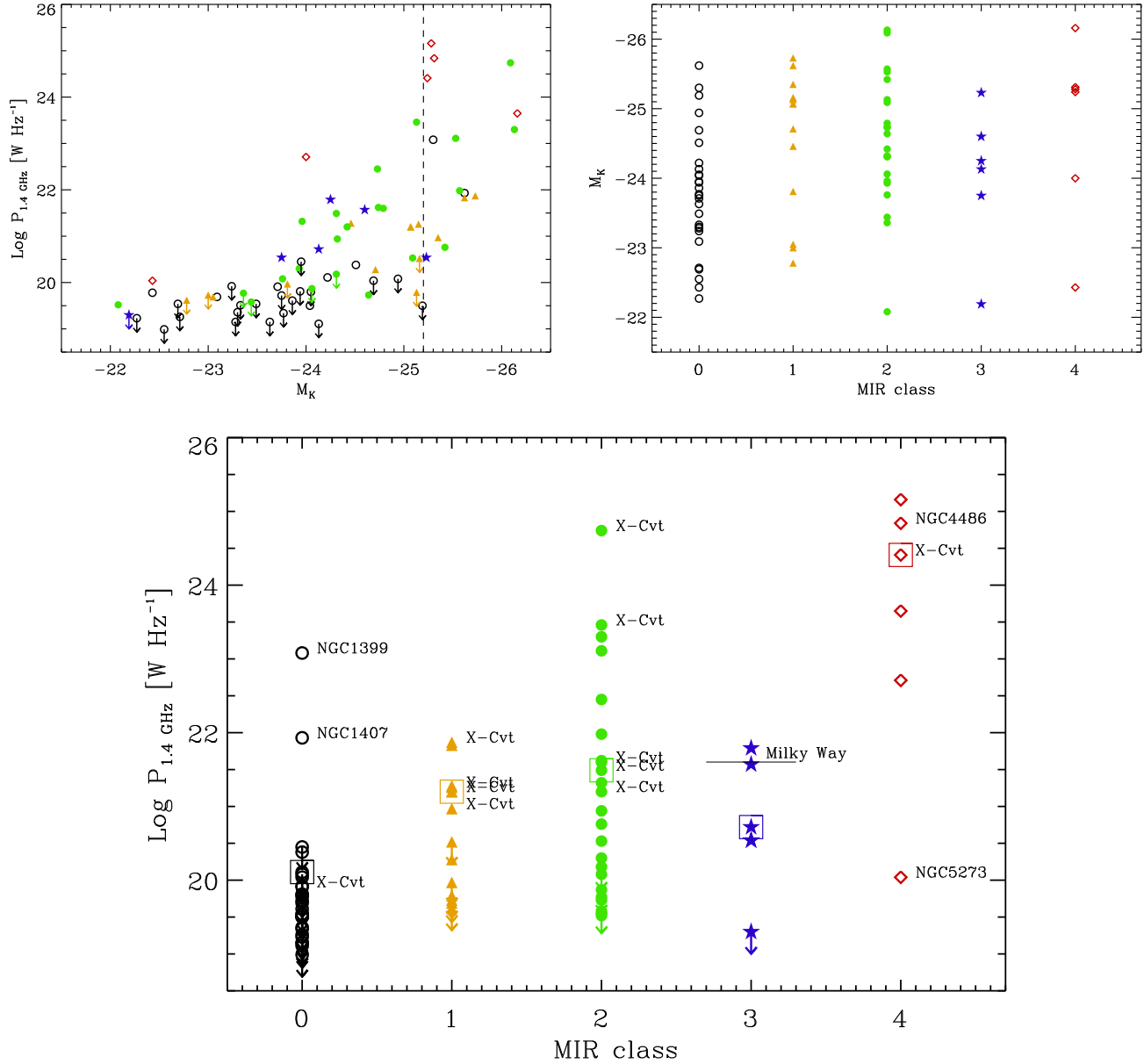
Figure 8. (*Top left*) 1.4 GHz radio power vs. M_K (open circle = class-0, triangle = class-1, full dot = class-2, star = class-3 and open diamond = class-4). Arrows represent upper limits. ETGs with $M_K \leqslant -25.2$, the vertical dashed line, are always detected (see Brown et al. 2011). (*Top right*) M_K vs. MIR class for the radio sample (see Table B1). (*Bottom*) The radio power vs. the MIR class. The radio power of the Milky Way is indicated with a horizontal line (see text). Large open squares represent the median value of the detected objects in each MIR class. ETGs with X-ray detected cavities (Cavagnolo et al. 2010) are labeled with X-Cvt.

Annibali, F., Bressan, A., Rampazzo, R., Zeilinger, W. W. 2006, A&A, 445, 79

Annibali, F., Bressan, A., Rampazzo, R. et al. 2007, A&A, 463, 455

Annibali, F., Bressan, A., Rampazzo, R., Zeilinger, W. W., Vega, O., Panuzzo, P. 2010, A&A, 519, A40

Armus, L., Charmandaris, V., Bernard-Salas, J., et al. 2007, ApJ, 656, 148

Athey, A., Bregman, J., Bregman, J., Temi, P., Sauvage, M. 2002, ApJ, 571, 272

Baldwin, J. A., Phillips, M. M., Terlevich, R. 1981, PASP, 93, 5

Bell, E.F. 2003, ApJ, 586, 794

Bekki, K. 2009, MNRAS, 339, 2221

Bertola, F., Galletta, G., Capaccioli, M., Rampazzo, R. 1988, A&A, 192, 24

Binette, L., Magris, C. G., Stasińska, G., Bruzual, A. G. 1994, A&A, 292, 13

Bois, M., Emsellem, E., Bournad, F. et al. 2012, MNRAS, 416, 1654

Boroson, B., Kim, D-W., Fabbiano, G. 2011, ApJ, 729, 12

Bregman, J. N., Temi, P., Bregman, J. D. 2006, ApJ, 647, 265

Bressan, A., Granato, G.L., Silva, L. 1998, A&A, 332, 135

Bressan, A., Panuzzo, P., Buson, L., Clemens, M., Granato, G. L., Rampazzo, R., Silva, L., Valdes, J. R., Vega, O., & Danese L. 2006, ApJ, 639, L55

Brandl, B. R., Bernard-Salas, J., Spoon, H. W. W, et al. 2006, ApJ, 653, 1129

Brown, M.J.I., Januzzi, B.T., Floyd, D.J.E., Mould, J.R. 2011, ApJL, 731, L41

Buson, L., Bressan, A., Panuzzo, P., Rampazzo, R., Valdés, J. R., Clemens, M., Marino, A., Chavez, M., Granato, G. L., Silva, L. 2009, ApJ, 705, 356

Capetti, A., Balmaverde, B. 2006, A&A, 453, 27

Cappellari, M., Emsellem, E., Krainović, D. et el. 2011, MNRAS, 413, 813

Cavagnolo, K.W., McNamara, B.R., Nulsen, P.E.J. et al. 2010, 720, 1066

Clemens, M.S., Bressan, A., Nikolic, B., Alexander, P., Annibali, F., Rampazzo, R. 2006, MNRAS, 370, 702

Clemens, M.S., Bressan, A., Nikolic, B., Rampazzo, R. 2009, MNRAS, 392, L35

Clemens, M. S., Jones, A. P., Bressan, A., Baes, M., Bendo, G. J. et al. 2010, A&A, 518, L50

Coccato, L., Corsini, E.M., Pizzella, A. et al. 2004, A&A, 416, 507

Corsini, E.M., Bertola, F. 1998, Journal of the Korean Physical Society, 33, 574

Dale, D. A., Smith, J. D. T., Armus, L. et al. 2006, ApJ, 646, 161

Davies, R. L., Efstathiou, G., Fall, S. M., Illingworth, G., Schechter, P. L. 1983, ApJ, 266, 41

de Vaucouleurs, G., de Vaucouleurs, A., Corwin, H.G. Jr. et al. 1991 *Third Reference Catalogue of Bright Galaxies*, Springer-Verlag, New York

Dopita, M. A., & Sutherland, R. S. 1995, ApJ, 455, 468

Draine, B.T., Li, A. 2007, ApJ, 657, 810

Dupraz C., Combes F. 1986, AAS, 166, 53

Elson, R. A. W., Fall, S. M., & Freeman, K. C. 1987, ApJ, 323, 54

Emsellem, E., Cappellari, M. Peletier, R. F., McDermid, R. M., Bacon, R. 2004, MNRAS, 352, 721

Emsellem, E., Cappellari, M., Krajnović, D., van de Ven, G., Bacon, R., et al. 2007, MNRAS, 379, 401.

Emsellem, E., Cappellari, M., Krajnović, D., Alatalo, K., Blitz, L. et al. 2011, MNRAS, 414, 888

Eracleous, M., Hwang, J. A., Flohic, H. M. L. G. 2010, ApJ, 711, 796

Fabian, A. C. 2012, Annu. Rev. Astron. Astrophys 50, 455

Feldmann, R., Carollo, C.M., Mayer, L. 2011, ApJ, 736, 88

Ferrari, F., Pastoriza, M. G., Macchetto, F., Caon, N. 2002, A&A, 136, 269

Finkelman, I., Brosch, N., Funes, J-G., et al. 2012, MNRAS, 422, 1384

Forbes, D. A. 1991, MNRAS, 249, 779

Gehrels N. 1986, ApJ, 303, 336

Gonzàlez-Martín, O., Masegosa, J., Márquez, I., Guainazzi, M., Jimènez-Baión, E. 2009, A&A, 506, 1107

Ghosh, K.K., Swartz, D. A., Tennant, A. F., Wu, K., Saripalli, L. 2005, ApJ, 623, 815

Goudfrooij, P., de Jong, T. 1995, A&A, 298, 784

Grützbauch, R., Trinchieri, G., Rampazzo, R., Held, E. V., Rizzi, L., Sulentic, J. W., Zeilinger, W. W. 2007, AJ, 133, 220

Heckman, T. M. 1980, A&A, 87, 152

Hernquist L., Quinn P. 1987a, ApJ, 312, 1

Henquist L., Quinn P. 1987b, ApJ, 312, 17

Ho, L. C., Filippenko, A. V., Sargent, W. L. W. 1997, ApJ, 487, 568

Kaneda, H., Onaka, T., Sakon, I. 2005, ApJ, 632, L83

Kaneda, H., Onaka, T., Kitayama, T., Okada, Y., Sakon, I. 2007, PASJ, 59, 107

Kaneda, H., Honaka, T., Sakon, L. et al. 2008, ApJ, 684, 270

Knapp, G. R., Guhathakurta, P., Kim, D-W., Jura, M. A. 1989, ApJS, 70, 329

Kormendy, J. 2004, Coevolution of Black Holes and Galaxies, 1

Kormendy, J.,Fisher, D.B., Cornell, M.E., Bender, R. 2009, ApJS, 182, 216

Koski, A. T., Osterbrock, D. E. 1976, ApJL, 203, L49

Krajnović, D. Bacon, R., Cappellari, M. et al. 2008, MNRAS, 390, 93

Lauer, T.R., Faber, S.M., Gehbardt K. et al. 2005, ApJ, 129, 2138

Longhetti, M., Bressan, A., Chiosi, C., Rampazzo, R. 2000, A&A, 353, 917

Lu, N., Helou, G., Werner, M.W. et al. 2003, ApJ, 588, 199

Macchetto, F., Pastoriza, M., Caon, N., Sparks, W. B., Giavalisco, M., Bender, R., & Capaccioli, M. 1996, A&A, 120, 463

Machacek, M.E., Jones, C., Forman, W.R. 2004, ApJ, 610, 813

Malin, D.F., Carter, D. 1983, ApJ, 274, 534

Maoz, D., Nagar, N. M., Falcke, H., Wilson, A. S. 2005, ApJ, 625, 699

Marigo, P., Girardi, L. 2007, A&A, 469, 239

Marino, A., Rampazzo, R., Bianchi, L. et al. 2011, MNRAS, 411, 311

Moore, B., Katz, N., Lake, G., Dressler, A., Oemler, A. 1996, Nature, 379, 613

Morganti, R., Holt, J., saripalli, L. et al. 2007, A&A, 476, 735

Morganti, R. 2010, PASA, 27 463

Morganti, R., Frieswijk, W., Oonk, R.J.B. et al. 2013 (arXiv:1302.2236v1)

Ocaña Flaquer, B., Combes, F., Leon, S., Lim, J 2010, A&A, 518, A9

Ogle, P., Antonucci, R., Appleton, P.N. et al. 2007, ApJ, 657, 161

Panuzzo, P., Vega, O., Bressan, A. et al. 2007, ApJ, 656, 206

Panuzzo, P., Rampazzo, R., Bressan, A., Vega, O., Annibali F., Buson, L.M., Clemens, M.S., Zeilinger, W.W. 2011, A&A, 528, A10

Patil, M. K., Pandey, S. K., Sahu, D. K., Kembhavi, A. 2007, A&A, 461, 103

Pellegrini, S. 2005, ApJ, 624, 155

Pellegrini, S. 2010, ApJ, 717, 640

Phillips, M. M., Jenkins, C. R., Dopita, M. A., Sadler, E. M., & Binette, L. 1986, AJ, 91, 1062

Pian, E., Romano, P., Maoz, D., Cucchiara, A., Pagani, C., Parola, V. L. 2010, MNRAS, 401, 677

Pierfederici, F., Rampazzo, R. 2004, AN, 325, 359

Pinkney, J., Gebhardt, K., Bender, R., Bower, G. Dressler, A. et al. 2003, ApJ, 596, 903

Pu, S. B., Saglia, R. P., Fabricius, M. H., Thomas, J., Ben-

der, R., Han, Z. 2010, A&A, 516, 4

Rampazzo, R., Annibali, F., Bressan, A., Longhetti, M., Padoan, F., Zeilinger, W. W. 2005, A&A, 433, 497

Rampazzo, R., 1988, A&A, 204, 81

Rampazzo, R., Annibali, F., Marino, A. et al. 2011, Ap&SS, 335, 201

Roussel, H. et al. 2007, ApJ, 669, 659

Sadler, E.M., Gerhard, O.E. 1995, MNRAS, 1985, 214, 177

Salomé, P., Combes, F., Edge, A.C., et al. 2006, A&A, 454, 437

Sandage, A., Tammann, G. A. 1987, Carnegie Institution of Washington Publication, Washigton: Carnegie Intistution 2nd edition

Sargsyan, L., Weedman, D., Lebouteiller, V., Houck, J., Barry, D., Hovhannisyan, A., Mickaelian, A. 2011, ApJ, 730, 19

Sarzi, M., Falcón-Barroso, J., Davies, R.L., Bacon, R., Bureau, M. et al. 2006, MNRAS, 366, 1151

Sarzi, M., Shields, J. C., Schawinski, K., Jeong, H., Shapiro, K., et al. 2010, MNRAS, 402, 2187

Serra, P., Trager, S. C., Oosterloo, T. A., & Morganti, R. 2008, A&A, 483, 57

Silchenko O.K., Moiseev, A. V., Afanasiev, V. L. 2009, ApJ, 694, 1550

Shankahr, F., Salucci, P., Danese, L., 2004, in "Baryons in Dark Matter Halos". Novigrad, Croatia, 5-9 Oct 2004. Editors: R. Dettmar, U. Klein, P. Salucci. Published by SISSA, Proceedings of Science, http://pos.sissa.it, p.59.1

Simões L., Ramiro D., Storchi-Bergmann, T. de Fátima S. M. Martini, P. 2007, ApJ, 655, 718

Smith, J.D.T., Drine, B.T., Dale, D.A. et al. 2007, ApJ, 656, 770

Smolcić, V., Rieckers, D.A. 2011, ApJ, 730, 64

Sofue, Y., Wakamatsu, K. 1993, PASJ, 45, 529

Stasińska, G., Vale Asari, N., Cid Fernandes, R., Gomes, J. M., Schlickmann, M., Mateus, A., Schoenell, W., Sodré, L., Jr. 2008, MNRAS, 391, L29

Tal, T. van Dokkum, P.G., Nelan, J., Bezanson, R. 2009, AJ, 138 1417

Temi, P., Brighenti, F., Mathews, W.G. 2007, ApJ, 666, 222

Thomson R.C. 1991, MNRAS, 253, 256

Thomson, R.C., Wright, 1990, MNRAS 224, 895

Thronson, H.A., Tacconi, L., Kenney, J. et al. 1989, ApJ, 344, 747

Tremblay, G. R., Chiaberge, M., Donzelli, C. J., Quillen, A. C., Capetti, A., Sparks, W. B., Macchetto, F. D. 2007, ApJ, 666, 109

Trinchieri, G., di Serego Alighieri, S. 1991, AJ, 101, 1647

Trinchieri, G., Goudfrooij, P. 2002, A&A, 386, 472

Tully, R. B. 1988, Nearby Galaxies Catalog (Cambridge: Cambridge Univ. Press)

Tully, B.R., Rizzi, L., Shaya, E. J., Courtois, H. M.; Makarov, D. I., Jacobs, B. A. 2009, AJ, 138, 323

Vega, O., Bressan, A., Panuzzo, P., Rampazzo, R., Clemens, M., Granato, G. L., Buson, L., Silva, L., Zeilinger, W. W. 2010, ApJ, 721, 1090

van Dokkum, P. G., Franx, M. 1995, AJ, 110, 2027

van Dokkum, P.G. 2005, AJ, 130, 2647

Van Verlzen, S., Falcke, H., Schellart, P. et al. 2012, A&A, in press

Véron-Cetty, M.-P., Véron, P. 1988, A&A, 204, 28

Verhoelst, T., van der Zypen, N., Hony, S. et al. 2009, A&A, 498, 127

Yan, R., Newman, J. A., Faber, S. M., Konidaris, N., Koo, D., & Davis, M. 2006, ApJ, 648, 281

Young, L. M., Bureau, M., Davis, T. A., Combes, F., McDermid, R. M. et al. (2011), MNRAS, 414, 940

Wall, J. V. 1977, unpublished lecture notes, Mullard Radio Astronomy Observatory, Cavendish Laboratory, Cambridge

Welch, G. A., Sage, L. J., Young, L. M. 2010, ApJ, 725, 100

Wiklind, T., Henkel, C. 2001, A&A, 375, 797

Whitmore B. C.; Lucas, R. A.; McElroy, D. B. et al. 1990, AJ, 100, 1489

Wrobel, J.M., Heeshen, D.S., 1988, ApJ, 335, 677

Wrobel, J. M., Heeschen, D. S. 1991, AJ, 101, 148

Zhang, Y., Gu, Q.-S., Ho, L.C. 2008, A&A, 487, 177

APPENDIX A: INTENSITIES OF PAH COMPLEXES, NEBULAR AND MOLECULAR EMISSIONS

Table A1 lists the intensity of PAH complexes of ETGs in the MIR spectral classes 2, 3 and 4. Table A2 lists the intensity of nebular and molecular line emission of ETGs in the MIR spectral classes 1, 2, 3 and 4. See Section 4 for details.

APPENDIX B: TABLES OF NUCLEAR PROPERTIES OF ETGS

We collect in Appendix B a set of tables summarizing the properties of ETGs used to characterize the MIR spectral classes in the atlas. References are reported in the caption of each table.

In Table B1 we report the optical "activity" class (columns 3 and 8), the nuclear ($2''$ radius) X-ray luminosity, $L_{X,nuc}$ (columns 4 and 9) and the radio power at 1.4 GHz (columns 5 and 10) which refers to the entire galaxy. In Table B2 and Table B3 we report the kinematical and morphological peculiarities (columns 3 and 4) for Es and S0s, respectively. In column 5 we give the morphology of dustlanes from optical observations. The kinematical peculiarities refer to the nuclear part of the galaxy, basically within one effective radius or less, so they provide a description of star and gas properties that contribute to the formation of the present *Spitzer*-IRS spectrum.

Table A1. PAH complex intensities.

Ident.	6.22μm (10⁻¹⁸ W m⁻²)	7.7μm[a] (10⁻¹⁸ W m⁻²)	8.6μm (10⁻¹⁸ W m⁻²)	11.3μm[b] (10⁻¹⁸ W m⁻²)	12.7μm[c] (10⁻¹⁸ W m⁻²)	17μm[d] (10⁻¹⁸ W m⁻²)
E						
NGC 1275	...	1047.2 ± 226.2	...	439.2 ± 141.9	794.2 ± 250.7	...
NGC 1297	13.3 ± 4.4	62.9 ± 3.3	13.8 ± 1.0	44.9 ± 1.4	21.8 ± 1.3	23.6 ± 2.5
NGC 1395	...	...	...	39.6 ± 3.4	27.6 ± 3.4	...
NGC 1453	...	77.4 ± 10.7	10.6 ± 2.4	31.0 ± 2.8	20.8 ± 2.1	13.2 ± 1.7
NGC 1549	...	...	...	9.6 ± 3.0	...	4.1 ± 1.1
NGC 2974	88.3 ± 9.4	409.7 ± 21.1	44.0 ± 3.9	256.9 ± 7.2	113.5 ± 5.7	144.9 ± 5.3
NGC 3258	113.8 ± 4.9	537.6 ± 15.3	110.4 ± 4.6	119.4 ± 3.1	72.0 ± 2.9	44.1 ± 1.4
NGC 3268	67.5 ± 6.4	341.1 ± 9.6	48.3 ± 2.9	150.5 ± 4.3	83.6 ± 4.1	73.3 ± 2.5
NGC 3557	32.5 ± 10.7	134.9 ± 11.5	19.6 ± 5.8	91.5 ± 4.9	48.4 ± 5.8	32.5 ± 3.9
NGC 3962	31.9 ± 8.8	133.1 ± 8.8	24.6 ± 3.8	102.8 ± 4.6	37.3 ± 2.9	35.3 ± 4.8
NGC 4261	40.4 ± 8.6	117.3 ± 13.8	11.6 ± 2.7	58.1 ± 4.9	53.6 ± 4.3	7.4 ± 1.3
NGC 4374	65.7 ± 20.6	258.3 ± 28.7	51.3 ± 6.6	178.9 ± 9.4	95.1 ± 7.0	65.2 ± 4.7
NGC 4486	...	89.6 ± 26.1	...	...	30.2 ± 9.7	...
NGC 4589	13.9 ± 4.2	52.5 ± 3.4	21.1 ± 1.1	49.8 ± 1.4	21.6 ± 2.1	27.7 ± 1.1
NGC 4696	...	...	...	11.3 ± 1.7	...	7.5 ± 0.5
NGC 4697	211.0 ± 21.2	816.8 ± 44.5	199.0 ± 16.2	263.0 ± 14.2	179.3 ± 5.0	78.4 ± 7.9
NGC 5018	232.1 ± 13.8	938.9 ± 39.4	233.7 ± 13.1	329.5 ± 11.9	152.1 ± 6.1	133.8 ± 7.1
NGC 5044	29.4 ± 7.0	112.5 ± 5.8	32.1 ± 3.1	58.1 ± 2.1	27.1 ± 1.8	28.8 ± 0.9
NGC 5077	...	66.6 ± 6.5	22.3 ± 4.7	30.8 ± 2.5	14.0 ± 1.8	41.2 ± 2.6
NGC 5090	13.5 ± 4.1	80.6 ± 13.4	10.5 ± 1.6	34.5 ± 2.4	21.8 ± 2.4	11.7 ± 3.1
IC 1459	...	108.4 ± 15.1	6.1 ± 1.8	84.9 ± 6.0	41.0 ± 5.4	47.1 ± 4.7
IC 3370	...	62.9 ± 19.6	13.1 ± 3.5	22.2 ± 3.6	22.5 ± 5.7	21.5 ± 2.5
IC 4296	...	...	...	26.7 ± 5.8	26.0 ± 5.6	19.8 ± 5.6
E/S0						
NGC 1052	120.0 ± 33.0	239.0 ± 41.4	...	195.8 ± 40.4	...	254.1 ± 66.3
NGC 4550	59.9 ± 5.3	323.2 ± 12.0	79.7 ± 5.1	102.9 ± 3.1	33.1 ± 2.1	...
NGC 4636	...	...	...	20.7 ± 5.0	...	8.8 ± 0.8
NGC 5353	...	52.5 ± 11.9	5.12 ± 1.1	27.4 ± 1.5	15.7 ± 1.2	13.9 ± 1.1
NGC 6868	50.5 ± 12.3	241.7 ± 24.3	27.5 ± 2.9	129.6 ± 6.9	86.8 ± 4.9	45.6 ± 3.1
S0						
NGC 1533	...	...	...	31.3 ± 3.8	12.6 ± 2.1	27.4 ± 1.9
NGC 1553	105.6 ± 10.3	406.8 ± 35.3	48.7 ± 7.4	275.8 ± 10.5	84.4 ± 7.0	78.3 ± 5.5
NGC 2685	...	128.9 ± 10.7	12.6 ± 1.4	85.6 ± 3.2	44.1 ± 3.1	41.6 ± 2.1
NGC 3245	1242.0 ± 47.1	4490.2 ± 85.2	567.7 ± 19.7	863.9 ± 23.3	439.4 ± 24.1	...
NGC 4036	106.4 ± 15.6	194.1 ± 11.6	42.9 ± 5.3	130.2 ± 4.1	75.9 ± 4.1	...
NGC 4371	...	55.2 ± 7.8	30.7 ± 7.2	21.3 ± 2.5	8.1 ± 1.5	5.1 ± 1.1
NGC 4383	3691.8 ± 81.7	12597.3 ± 158.3	2985.3 ± 72.8	2710.8 ± 65.4	1486.1 ± 38.1	563.2 ± 56.9
NGC 4435	1304.5 ± 29.1	5906.7 ± 86.7	805.1 ± 21.5	1035.7 ± 23.7	802.2 ± 31.8	357.6 ± 15.3
NGC 4477	104.4 ± 14	278.6 ± 12.6	25.6 ± 1.9	133.7 ± 4.1	59.3 ± 2.8	64.7 ± 2.1
NGC 4552	...	...	...	38.3 ± 7.9	...	7.9 ± 1.8
NGC 5128	3337.4 ± 295.6	18734.1 ± 909.5	$>1569.1 \pm 330.6$	$>5603.1 \pm 511.2$	4251.8 ± 715.7	5230.6 ± 461.3
NGC 5273	...	346.2 ± 12.9	279.1 ± 15.1	329.5 ± 10.1	97.4 ± 5.5	320.6 ± 16.1
NGC 5631	...	87.3 ± 3.4	31 ± 1.1	45.5 ± 2.1	21.8 ± 2.1	28.9 ± 2.1
NGC 5898	...	53 ± 16.3	...	46.5 ± 4.3	15.1 ± 3.3	21.7 ± 2.4
IC 5063	...	1190.4 ± 140.9	208.8 ± 68.9	462.9 ± 125.4	...	...

Notes. Uncertainties are 1σ. [a] Includes the 7.42 μm, 7.60 μm and the 7.85 μm features. [b] Includes the 11.23 μm, and the 11.33 μm features. [c] Includes the 12.62 μm and the 12.69 μm features. [d] Includes the 16.45 μm, 17.04 μm, 17.375 μm and the 17.87 μm features. We consider the 8.6 μm and 11.3μm PAH emissions in NGC 5128 as lower limits because of the huge silicate absorption.

This paper has been typeset from a TeX/ LaTeX file prepared by the author.

Table A2. Nebular and molecular emission line intensities

Galaxy name	H$_2$ 0–0 S(7) 5.51 μm	H$_2$ 0–0 S(6) 6.11 μm	H$_2$ 0–0 S(5) 6.91 μm	[ArII] 6.99 μm	H Pfα 7.46 μm	H$_2$ 0–0 S(4) 8.03 μm	[ArIII] 8.99 μm	H$_2$ 0–0 S(3) 9.66 μm	[SIV] 10.51 μm	H$_2$ 0–0 S(2) 12.28 μm
E										
NGC 1209	...	...	...	4.8 ± 1.0	...	...	3.5 ± 0.9	...	...	1.4 ± 0.2
NGC 1275	120.4 ± 31.9	...	194.4 ± 25.0	128.7 ± 18.4	...	...	...	184.9 ± 35.5	...	...
NGC 1297	...	...	2.8 ± 0.3	3.3 ± 0.3	...	0.5 ± 0.1	1.2 ± 0.3	5.1 ± 0.5	0.6 ± 0.2	2.1 ± 0.1
NGC 1395	...	...	...	...	...	...	...	...	...	1.8 ± 0.4
NGC 1404	...	...	...	...	...	...	...	...	...	...
NGC 1453	...	8.5 ± 1.7	...	9.0 ± 1.1	3.9 ± 0.6	...	...	7.1 ± 1.7	2.2 ± 1.0	1.1 ± 0.2
NGC 1549	...	...	...	...	...	...	...	...	...	...
NGC 1700	...	...	...	...	...	...	...	...	...	...
NGC 2974	9.0 ± 2.5	3.8 ± 0.5	16.1 ± 0.8	18.7 ± 1.4	...	4.2 ± 0.3	...	30.9 ± 1.7	4.1 ± 0.6	13.3 ± 0.8
NGC 3258	...	...	4.1 ± 0.3	8.5 ± 0.5	...	2.3 ± 0.1	0.8 ± 0.1	5.1 ± 0.8	0.7 ± 0.2	4.2 ± 0.2
NGC 3268	...	...	6.1 ± 0.6	7.7 ± 0.5	...	1.6 ± 0.1	0.5 ± 0.1	4.5 ± 0.7	1.6 ± 0.3	2.4 ± 0.2
NGC 3557	...	...	...	5.4 ± 0.6	...	...	...	...	...	...
NGC 3962	...	...	3.1 ± 0.7	8.6 ± 1.0	...	4.5 ± 0.4	2.5 ± 0.7	16.6 ± 1.5	2.2 ± 0.6	4.8 ± 0.3
NGC 4261	...	...	6.6 ± 1.1	12.4 ± 1.3	...	...	3.3 ± 1.1	5.2 ± 1.7	4.2 ± 1.0	5.3 ± 0.4
NGC 4374	...	...	7.4 ± 1.0	24.4 ± 2.2	...	1.3 ± 0.1	6.9 ± 1.5	8.3 ± 2.0	5.2 ± 1.2	3.6 ± 0.5
NGC 4486	...	...	...	36.0 ± 3.0	...	...	8.2 ± 2.6	...	...	...
NGC 4589	1.4 ± 0.4	...	...	1.1 ± 0.3	...	...	1.0 ± 0.3	...	...	...
NGC 4696	...	...	3.5 ± 0.8	8.4 ± 0.9	...	...	...	6.4 ± 0.9	...	1.5 ± 0.1
NGC 4697	14.5 ± 3.2	8.2 ± 1.1	7.4 ± 1.2	12.9 ± 1.1	0.3 ± 0.1	6.4 ± 0.5	8.2 ± 1.2	8.2 ± 2.0	...	1.6 ± 0.1
NGC 5011	...	...	...	7.2 ± 1.0	...	...	2.1 ± 0.6	3.6 ± 0.6	1.8 ± 0.5	...
NGC 5018	...	6.3 ± 1.0	7.5 ± 1.0	9.6 ± 1.0	...	4.3 ± 0.4	3.4 ± 0.5	4.9 ± 1.6	...	4.7 ± 0.5
NGC 5044	6.4 ± 1.3	1.8 ± 0.4	14.9 ± 0.9	14.6 ± 0.5	...	2.9 ± 0.2	1.8 ± 0.3	23.4 ± 1.1	1.2 ± 0.3	10.6 ± 0.4
NGC 5077	...	...	6.2 ± 1.1	9.1 ± 0.8	3.5 ± 0.6	1.7 ± 0.2	2.6 ± 0.6	9.4 ± 0.9	1.2 ± 0.5	2.8 ± 0.4
NGC 5090	...	3.5 ± 0.9	7.0 ± 0.6	9.2 ± 0.8	...	1.8 ± 0.2	3.0 ± 0.8	...	3.1 ± 0.5	...
NGC 5813	...	7.5 ± 1.5	6.4 ± 0.6	15.3 ± 1.3	...	2.9 ± 0.4	3.6 ± 1.0	6.3 ± 0.9	...	...
NGC 7619	...	...	...	...	...	...	...	...	...	...
IC 1459	...	...	5.0 ± 1.6	21.2 ± 1.5	...	...	...	10.3 ± 2.4	...	2.6 ± 0.5
IC 2006	...	...	...	...	...	...	...	...	...	...
IC 3370	...	...	4.2 ± 0.3	4.8 ± 0.4	...	...	2.3 ± 0.3	3.7 ± 0.4	...	2.2 ± 0.2
IC 4296	...	...	...	...	...	...	...	...	...	2.2 ± 0.5
E/S0										
NGC 1052	17.8 ± 3.1	8.7 ± 2.7	31.5 ± 7.8	81.0 ± 2.7	...	6.7 ± 2.0	17.0 ± 2.9	63.3 ± 10.7	...	11.2 ± 3.9
NGC 4472	...	...	3.1 ± 1.0	11.3 ± 2.5	...	...	...	...	...	...
NGC 4550	...	2.0 ± 0.4	3.4 ± 0.4	2.7 ± 0.3	...	...	1.3 ± 0.2	6.4 ± 0.6	1.9 ± 0.4	2.4 ± 0.3
NGC 4636	...	...	...	...	...	...	...	...	...	...
NGC 5353	...	...	...	...	...	...	...	2.0 ± 0.6	...	1.1 ± 0.1
NGC 6868	7.0 ± 2.0	3.5 ± 1.0	20.2 ± 1.4	16.3 ± 1.0	...	6.0 ± 0.5	4.0 ± 0.6	23.9 ± 1.5	1.4 ± 0.4	8.9 ± 0.3
S0										
NGC 584	...	...	...	...	...	...	...	...	...	...
NGC 1366	...	...	...	...	...	...	...	...	...	...
NGC 1533	...	...	...	2.2 ± 0.5	3.8 ± 1.2	...	...	3.6 ± 0.7	...	1.8 ± 0.4
NGC 1553	...	1.5 ± 0.3	5.9 ± 0.8	10.6 ± 1.2	...	3.7 ± 0.4	...	10.8 ± 2.7	3.7 ± 0.8	6.2 ± 0.6
NGC 2685	...	...	...	7.6 ± 1.0	2.3 ± 0.6	2.4 ± 0.3	4.2 ± 0.9	7.9 ± 1.0	3.0 ± 0.6	2.7 ± 0.3
NGC 3245	...	...	25.0 ± 1.5	36.8 ± 1.8	18.1 ± 8.0	...	...	...	...	...
NGC 4036	...	24.6 ± 3.0	20.5 ± 1.2	7.5 ± 1.1	...	10.6 ± 1.0	8.8 ± 1.2	35.7 ± 2.1	1.5 ± 0.4	13.8 ± 1.0
NGC 4371	...	...	...	...	...	...	...	...	...	1.2 ±0.3
NGC 4382	...	...	...	...	...	...	...	...	...	...
NGC 4383	...	...	...	91.3 ± 5.0	...	...	83.1 ± 3.1	...	81.3 ± 17.2	...
NGC 4435	...	...	25.0 ± 1.5	40.0 ± 2.0	...	22.2 ± 2.0	...	...	...	...
NGC 4477	...	4.0 ± 1.0	9.0 ± 1.0	18.9 ± 1.3	...	3.2 ± 0.4	4.9 ± 0.7	12.8 ± 1.7	2.9 ± 0.7	7.0 ± 0.5
NGC 4552	...	...	...	...	...	...	...	10.4 ± 3.4	...	2.8 ± 0.9
NGC 4649	...	...	...	...	...	...	...	...	...	...
NGC 5128	...	83.4 ± 22.2	246.6 ± 40.2	804.3 ± 92.9	...	54.5 ± 8.9	82.9 ± 26.2	231.7 ± 71.3	...	213.7 ± 69.3
NGC 5273	...	...	...	...	...	22.9 ± 2.0	...	...	30.4 ± 8.0	9.5 ± 0.8
NGC 5631	...	...	6.3 ± 1.3	3.8 ± 1.0	5.9 ± 1.2	...	3.4 ± 1.1	11.0 ± 1.5	...	0.6 ± 0.1
NGC 5846	...	...	...	...	...	...	...	0.5 ± 0.1	...	0.6 ± 0.1
NGC 5898	...	...	...	...	...	...	...	4.1 ± 1.4	...	0.9 ± 0.2
NGC 7192	...	...	...	2.6 ± 0.8	...	...	...	...	...	...
NGC 7332	...	...	...	...	...	...	...	3.9 ± 0.2	...	...
IC 5063	...	...	133.8 ± 27.7	106.5 ± 29.6	...	...	176.3 ± 44.8	244.9 ± 49.9	788.5 ± 123.9	...

Notes. Uncertainties are 1σ. Values are in unit of 10^{-18} [W m^{-2}]. Neither atomic nor molecular emission lines are detected in Passive ETGs. [d] The two lines are blended in LL1 spectra: the values reported are the result of a line de-blending.

Table A2. Nebular and molecular emission line intensities (*cont.*)

Galaxy name	[NeII] 12.81 μm	[NeV] 14.32 μm	[NeIII] 15.55 μm	H$_2$ 0–0 S(1) 17.03 μm	[FeII] 17.94 μm	[SIII] 18.71 μm	[ArIII] 21.83 μm	[NeV] 24.32 μm	[OIV]^d 25.89 μm	[FeII]^d 25.99 μm
E										
NGC 1209	3.1 ± 0.3	...	3.0 ± 0.2	...	0.9 ± 0.1	1.5 ± 0.1	...	...	0.4 ± 0.1	2.1 ± 0.2
NGC 1275	507.1 ± 50.1	...	398.6 ± 98.8	...	...	...	...	...	...	...
NGC 1297	1.9 ± 0.1	...	1.2 ± 0.1	7.5 ± 0.2	...	0.4 ± 0.1	...	...	0.8 ± 0.1	1.0 ± 0.1
NGC 1395	2.8 ± 0.2	...	...	...	...	...	...	...	...	...
NGC 1404	5.9 ± 2.0	...	4.3 ± 1.5	...	...	...	...	...	...	...
NGC 1453	3.6 ± 0.4	...	7.5 ± 0.5	2.2 ± 0.2	...	2.3 ± 0.3	...	...	...	...
NGC 1549	2.5 ± 0.4	...	4.4 ± 0.5	0.8 ± 0.2	...	1.6 ± 0.4	...	...	...	...
NGC 1700	...	...	2.8 ± 0.9	...	...	...	...	...	...	...
NGC 2974	35.0 ± 1.0	...	27.5 ± 1.2	21.8 ± 1.1	...	13.3 ± 0.9	...	7.3 ± 0.9	2.1 ± 0.2	10.3 ± 0.6
NGC 3258	15.2 ± 0.5	...	4.6 ± 0.3	6.6 ± 0.3	1.2 ± 0.2	3.7 ± 0.3	2.2 ± 0.5	...	1.1 ± 0.2	1.8 ± 0.4
NGC 3268	10.5 ± 0.4	...	5.5 ± 0.2	3.0 ± 0.3	1.0 ± 0.3	3.4 ± 0.2	1.3 ± 0.2	...	1.0 ± 0.1	1.9 ± 0.2
NGC 3557	9.6 ± 0.6	...	9.0 ± 0.6	...	1.4 ± 0.2	2.7 ± 0.3	...	1.1 ± 0.3	0.8 ± 0.1	2.8 ± 0.3
NGC 3962	14.2 ± 0.4	1.0 ± 0.1	8.2 ± 0.5	4.7 ± 0.2	2.8 ± 0.2	5.3 ± 0.2	...	...	3.1 ± 0.2	3.0 ± 0.2
NGC 4261	31.7 ± 1.6	1.7 ± 0.4	11.6 ± 0.8	...	...	1.3 ± 0.3	...	...	...	...
NGC 4374	32.9 ± 1.3	1.6 ± 0.3	26.5 ± 1.1	8.3 ± 0.6	1.7 ± 0.3	14.9 ± 0.5	2.5 ± 0.6	...	3.5 ± 0.3	5.7 ± 0.6
NGC 4486	58.3 ± 2.8	...	24.1 ± 2.7	...	...	19.1 ± 3.1	...	...	...	...
NGC 4589	0.4 ± 0.1	...	0.3 ± 0.1	0.3 ± 0.1	...	0.3 ± 0.1	...	...	...	...
NGC 4696	13.3 ± 0.6	...	7.6 ± 0.3	6.4 ± 0.3	...	1.2 ± 0.1	...	...	1.5 ± 0.1	2.8 ± 0.2
NGC 4697	8.3 ± 0.6	...	9.1 ± 1.1	4.0 ± 0.5	...	5.8 ± 0.8	...	...	...	...
NGC 5011	2.8 ± 0.3	0.6 ± 0.2	3.9 ± 0.3	...	...	1.8 ± 0.1	...	...	0.9 ± 0.1	0.5 ± 0.1
NGC 5018	19.7 ± 1.0	...	15.9 ± 1.0	7.3 ± 0.4	...	6.0 ± 0.7	...	...	2.5 ± 0.4	3.1 ± 0.7
NGC 5044	24.3 ± 0.9	...	12.2 ± 0.4	13.4 ± 0.5	0.6 ± 0.1	3.1 ± 0.2	1.0 ± 0.2	1.2 ± 0.2	1.5 ± 0.1	2.1 ± 0.2
NGC 5077	20.6 ± 1.0	0.6 ± 0.1	17.9 ± 0.8	12.7 ± 0.7	1.4 ± 0.2	6.3 ± 0.4	2.9 ± 0.6	...	1.7 ± 0.1	8.4 ± 0.5
NGC 5090	20.7 ± 0.6	0.9 ± 0.2	9.4 ± 0.6	1.6 ± 0.3	3.8 ± 0.4	4.0 ± 0.3	4.1 ± 0.4	...	2.7 ± 0.3	2.2 ± 0.2
NGC 5813	6.3 ± 0.3	...	7.0 ± 0.3	2.3 ± 0.4	...	3.0 ± 0.2	...	...	...	...
NGC 7619	...	...	1.4 ± 0.6	...	...	...	...	...	...	...
IC 1459	51.4 ± 2.1	...	38.7 ± 1.7	1.4 ± 0.3	3.6 ± 0.6	9.9 ± 0.7	...	4.7 ± 1.1	2.8 ± 0.3	12.3 ± 1.0
IC 2006	...	...	3.4 ± 1.6	...	...	...	...	...	...	...
IC 3370	2.1 ± 0.1	...	1.4 ± 0.1	4.4 ± 0.2	...	0.6 ± 0.1	...	0.3 ± 0.1	0.7 ± 0.1	0.9 ± 0.1
IC 4296	24.1 ± 1.4	0.5 ± 0.1	10.9 ± 0.7	1.7 ± 0.5	1.4 ± 0.3	4.2 ± 0.6	...	...	3.9 ± 0.4	2.9 ± 0.2
E/S0										
NGC 1052	250.3 ± 9.7	...	180.4 ± 9.3	47.5 ± 9.7	43.6 ± 12.6	71.4 ± 9.4	...	...	27.2 ± 3.9	50.1 ± 9.3
NGC 4472	2.7 ± 0.7	...	...	...	...	...	...	...	...	...
NGC 4550	4.3 ± 0.3	...	...	...	...	...	...	...	...	...
NGC 4636	12.9 ± 0.8	...	15.1 ± 0.8	2.4 ± 0.4	...	6.1 ± 0.5	...	...	...	...
NGC 5353	2.5 ± 0.2	...	3.3 ± 0.3	2.1 ± 0.1	...	1.7 ± 0.2	...	...	0.7 ± 0.1	1.8 ± 0.2
NGC 6868	30.0 ± 1.0	1.1 ± 0.1	23.8 ± 0.8	9.6 ± 0.6	1.5 ± 0.2	7.8 ± 0.4	1.3 ± 0.4	2.0 ± 0.4	4.8 ± 0.3	6.6 ± 0.4
S0										
NGC 584	3.1 ± 1.0	...	6.5 ± 0.7	...	...	...	...	...	...	...
NGC 1366	1.9 ± 0.4	...	3.4 ± 0.4	...	...	1.7 ± 0.2	...	...	0.5 ± 0.1	0.5 ± 0.1
NGC 1533	5.3 ± 0.3	...	6.6 ± 0.4	4.5 ± 0.2	...	5.7 ± 0.4	1.6 ± 0.2	...	0.6 ± 0.1	3.0 ± 0.3
NGC 1553	25.1 ± 0.9	0.4 ± 0.1	22.3 ± 1.6	5.7 ± 0.5	...	8.5 ± 0.9	...	...	1.3 ± 0.2	6.1 ± 0.9
NGC 2685	8.6 ± 0.5	...	6.9 ± 0.4	5.2 ± 0.3	...	0.5 ± 0.1	...	...	1.4 ± 0.2	2.4 ± 0.2
NGC 3245	104.6 ± 13.6	...	...	...	...	...	...	...	...	...
NGC 4036	34.2 ± 1.4	...	...	...	...	...	...	...	...	...
NGC 4371	1.8 ± 0.2	...	0.7 ± 0.2	...	...	...	...	...	...	...
NGC 4382	...	...	3.4 ± 0.9	...	...	...	...	...	...	...
NGC 4383	359 ± 11.1	...	373.0 ± 16.3	24.6 ± 8.0	...	305.5 ± 19.3	...	...	26.9 ± 7.6	25.6 ± 8.0
NGC 4435	85.9 ± 2.3	...	22.2 ± 2.6	17.6 ± 2.2	...	22.4 ± 1.7	...	...	...	...
NGC 4477	20.2 ± 1.0	1.1 ± 0.3	19.7 ± 1.0	12.8 ± 0.6	1.5 ± 0.2	9.3 ± 0.4	...	...	4.5 ± 0.4	5.6 ± 0.4
NGC 4552	13.5 ± 1.1	0.3 ± 0.1	10.4 ± 1.1	...	...	10.0 ± 1.0	...	...	...	...
NGC 4649	2.2 ± 0.8	...	3.7 ± 0.8	...	...	...	...	...	...	...
NGC 5128	2057.8 ± 118.1	201.4 ± 64.2	1297.1 ± 148.6	634.7 ± 60.2	...	710.9 ± 62.2	...	...	541.3 ± 75.3	551.3 ± 109.2
NGC 5273	27.0 ± 1.3	...	16.4 ± 1.6	7.5 ± 1.2	...	9.7 ± 1.5	...	...	...	...
NGC 5631	3.4 ± 0.1	...	3.2 ± 0.1	4.6 ± 0.2	...	1.0 ± 0.1	...	2.4 ± 0.2	1.4 ± 0.1	1.7 ± 0.1
NGC 5846	12.5 ± 0.9	...	9.1 ± 0.6	2.0 ± 0.2	...	3.8 ± 0.3	...	...	...	...
NGC 5898	4.2 ± 0.3	...	8.3 ± 0.5	3.1 ± 0.3	...	3.8 ± 0.4	...	1.2 ± 0.4	0.5 ± 0.1	2.1 ± 0.2
NGC 7192	2.4 ± 0.4	...	1.0 ± 0.2	0.3 ± 0.1	0.3 ± 0.1	0.3 ± 0.1	1.0 ± 0.2	...	...	0.6 ± 0.1
NGC 7332	...	...	9.0 ± 0.9	1.7 ± 0.3	...	3.4 ± 0.5	...	1.2 ± 0.4	3.4 ± 0.2	4.7 ± 0.3
IC 5063	238.7 ± 48.2	335.2 ± 68.7	1103.6 ± 88.9	168.1 ± 36.9	...	321.7 ± 71.2	...	402.8 ± 107.1	477.1 ± 44.8	673.0 ± 51.4

Table A2. Nebular and molecular emission line intensities (*cont.*)

Galaxy name	H$_2$ 0–0 S(0) 28.22 μm	[SIII] 33.48 μm	[SiII] 34.82 μm	[FeII] 35.35 μm	[NeIII] 36.01 μm
E					
NGC 1209	...	3.5 ± 0.2	11.3 ± 0.3	...	1.1 ± 0.1
NGC 1275	...	456.0 ± 122.0	847.4 ± 127.8	...	...
NGC 1297	3.0 ± 0.1	1.5 ± 0.1	5.5 ± 0.2	0.3 ± 0.1	...
NGC 1395	...	...	...	...	...
NGC 1404	...	...	...	...	...
NGC 1453	...	...	...	...	...
NGC 1549	...	...	...	...	...
NGC 1700	...	...	...	...	...
NGC 2974	2.6 ± 0.6	13.5 ± 1.2	44.9 ± 1.2	...	...
NGC 3258	...	5.6 ± 0.5	...	...	...
NGC 3268	...	4.8 ± 0.3	7.6 ± 0.5	...	...
NGC 3557	...	8.4 ± 0.4	7.1 ± 0.4	2.7 ± 0.3	4.3 ± 0.3
NGC 3962	...	6.2 ± 0.5	31.7 ± 1.0	1.4 ± 0.4	2.1 ± 0.3
NGC 4261	2.7 ± 0.9	9.3 ± 1.1	...	...	...
NGC 4374	2.2 ± 0.6	24.3 ± 1.0	40.8 ± 1.3	3.6 ± 0.7	...
NGC 4486	...	...	...	...	...
NGC 4589	...	0.3 ± 0.1	0.4 ± 0.1	...	...
NGC 4696	0.9 ± 0.1	4.9 ± 0.2	14.5 ± 0.5	4.0 ± 0.1	4.5 ± 0.2
NGC 4697	...	...	...	...	...
NGC 5011	...	3.1 ± 0.2	5.0 ± 0.2	...	...
NGC 5018	...	12.1 ± 2.7	18.3 ± 3.8	...	...
NGC 5044	1.5 ± 0.2	9.0 ± 0.3	44.4 ± 1.1	0.8 ± 0.1	1.4 ± 0.1
NGC 5077	2.6 ± 0.5	11.7 ± 0.6	45.6 ± 1.4	2.1 ± 0.5	1.6 ± 0.5
NGC 5090	0.8 ± 0.2	5.3 ± 0.4	12.9 ± 0.5	...	...
NGC 5813	...	...	...	...	...
NGC 7619	...	...	...	...	...
IC 1459	3.1 ± 1.0	23.5 ± 1.7	50.0 ± 2.2	...	...
IC 2006	...	...	...	...	...
IC 3370	0.7 ± 0.1	1.6 ± 0.2	0.9 ± 0.2	1.5 ± 0.2	...
IC 4296	...	10.1 ± 1.1	15.0 ± 0.8	2.0 ± 0.5	...
E/S0					
NGC 1052	...	84.6 ± 13.3	207.3 ± 18.4	...	...
NGC 4472	...	...	...	...	...
NGC 4550	...	...	...	...	...
NGC 4636	...	...	...	...	...
NGC 5353	0.8 ± 0.2	1.0 ± 0.3	3.4 ± 0.3	2.8 ± 0.4	2.9 ± 0.4
NGC 6868	...	22.3 ± 0.8	28.8 ± 1.0	2.8 ± 0.5	3.8 ± 0.5
S0					
NGC 584	...	...	...	...	...
NGC 1366	...	1.5 ± 0.1	2.7 ± 0.2	1.5 ± 0.2	...
NGC 1533	1.8 ± 0.3	6.3 ± 0.4	12.0 ± 0.4	0.5 ± 0.1	...
NGC 1553	...	15.4 ± 1.0	28.9 ± 1.8	...	7.5 ± 0.7
NGC 2685	1.7 ± 0.2	3.8 ± 0.3	12.9 ± 0.5	...	...
NGC 3245	...	...	...	...	...
NGC 4036	...	...	...	...	...
NGC 4371	...	...	...	...	...
NGC 4382	...	...	...	...	...
NGC 4383	...	459.9 ± 38.7	390.9 ± 26.8	...	...
NGC 4435	...	...	...	...	...
NGC 4477	...	16.8 ± 1.1	31.4 ± 1.5	...	...
NGC 4552	...	...	...	...	...
NGC 4649	...	...	...	...	...
NGC 5128	...	234.9 ± 77.3	...	...	...
NGC 5273	...	49.5 ± 4.1	83.2 ± 5.8	...	...
NGC 5631	1.7 ± 0.5	3.6 ± 0.2	9.4 ± 0.1	3.7 ± 0.3	...
NGC 5846	...	...	...	...	...
NGC 5898	...	4.5 ± 0.4	9.3 ± 0.5	...	2.0 ± 0.4
NGC 7192	...	2.7 ± 0.2	4.0 ± 0.2	...	...
NGC 7332	1.8 ± 0.3	4.7 ± 0.3	8.2 ± 0.7	1.0 ± 0.3	1.1 ± 0.2
IC 5063	...	480.5 ± 58.9	524.9 ± 66.5	...	...

Table B1. Optical activity class, nuclear X-ray luminosity and 1.4 GHz radio power

Ident.	Morpho. RSA	Opt. class	Log $L_{X,nuc}$ [erg s^{-1}]	$P_{1.4\ GHz}$ [W Hz^{-1}]	Ident.	Morpho. RSA	Opt. class	Log $L_{X,nuc}$ [erg s^{-1}]	$P_{1.4\ GHz}$ [W Hz^{-1}]
NGC 636	E1	...	...	$<6.4\ 10^{19}$	NGC 5090	E2	LIN(H)	...	...
NGC 720	E5	...	38.90	$<1.2\ 10^{20}$	NGC 5638	E1	IN	...	$<4.1\ 10^{19}$
NGC 821	E6	...	<38.37	$<6.3\ 10^{19}$	NGC 5812	E0	IN	...	$1.3\ 10^{20}$
NGC 1209	E6	LIN(H)	...	$1.9\ 10^{21}$	NGC 5813	E1	LIN(W); L2:	38.80	$1.8\ 10^{21}$
NGC 1275	E pec	S1.5	...	$1.4\ 10^{25}$	NGC 5831	E4	IN	...	$<5.3\ 10^{19}$
NGC 1297	E2	LIN(H)	...	$<5.9\ 10^{19}$	NGC 7619	E3	...	40.84	$6.8\ 10^{21}$
NGC 1339	E4	...	...	$<4.2\ 10^{19}$	IC 1459	E1	LIN(H)	40.87	$1.3\ 10^{23}$
NGC 1374	E0	...	...	$<2.3\ 10^{19}$	IC 2006	E1	Comp(W)	...	$4.9\ 10^{19}$
NGC 1379	E0	...	...	$<1.4\ 10^{19}$	IC 3370	E2 pec	LIN(H)	...	$8.8\ 10^{20}$
NGC 1395	E2	...	39.06	$5.4\ 10^{19}$	IC 4296	E0	LIN(H)	41.20	$5.6\ 10^{24}$
NGC 1399	E1		<38.96	$1.2\ 10^{23}$					
NGC 1404	E2	...	40.57	$1.9\ 10^{20}$	NGC 1052	E3/S0	LIN(H); L1.9	41.20	$5.1\ 10^{22}$
NGC 1407	E0	IN	<39.14	$8.7\ 10^{20}$	NGC 1351	S0$_1$/E6	...	...	$4.9\ 10^{19}$
NGC 1426	E4	IN	...	$<8.5\ 10^{19}$	NGC 4472	E1/S0$_1$	S2::	<38.67	$7.4\ 10^{21}$
NGC 1427	E5	...	...	$<3.2\ 10^{19}$	NGC 4550	E/S0	L2	<38.37	$<2.0\ 10^{19}$
NGC 1453	E2	LIN(H)	...	$9.5\ 10^{21}$	NGC 4570	E7/S0$_1$	...	38.18	$<3.5\ 10^{19}$
NGC 1549	E2	...	38.46	...	NGC 4636	E0/S0$_1$	LIN(H); L1.9	<38.24	$2.0\ 10^{21}$
NGC 1700	E3	...	38.84	$<3.3\ 10^{20}$	NGC 5353	S0$_1$/E7	L2/T2	...	$4.2\ 10^{21}$
NGC 2300	E3	...	40.96	$2.4\ 10^{20}$	NGC 6868	E3/S0$_{2/3}$	LIN(H)	...	...
NGC 2974	E4	LIN(H)	40.32	$5.7\ 10^{20}$	NGC 584	S0$_1$	...	...	$1.6\ 10^{21}$
NGC 3193	E2	L2:	<39.74	$<1.1\ 10^{20}$	NGC 1366	S0$_1$	IN	...	...
NGC 3258	E1	Comp(H)	...	$6.2\ 10^{21}$	NGC 1389	S0$_1$/SB0$_1$	IN	...	$<5.4\ 10^{19}$
NGC 3268	E2	LIN(H)	...	$3.7\ 10^{21}$	NGC 1533	SB0$_2$/SBa	LIN(H)	...	...
NGC 3377	E6	...	38.24	$<1.8\ 10^{19}$	NGC 1553	S0$_{1/2}$ pec	LIN(W)	40.22	...
NGC 3379	E0	L2/T2::	38.12	$3.2\ 10^{19}$	NGC 2685	S0$_3$ pec	S2/T2	...	$3.3\ 10^{19}$
NGC 3557	E3	LIN(W)	40.24	$2.0\ 10^{23}$	NGC 3245	S0$_1$	T2:	39.00	$3.5\ 10^{20}$
NGC 3608	E1	L2/S2:	38.21	$8.2\ 10^{19}$	NGC 4036	S0$_3$/Sa	L1.9	39.05	$5.4\ 10^{20}$
NGC 3818	E5	IN(Traces)	...	$<2.8\ 10^{20}$	NGC 4339	S0$_{1/2}$	...	...	$<9.7\ 10^{18}$
NGC 3904	E2	...	...	$<1.3\ 10^{20}$	NGC 4371	SB0$_{2/3}$(r)	...	...	$<3.8\ 10^{19}$
NGC 3962	E1	LIN(H)	...	$3.4\ 10^{20}$	NGC 4377	S0$_1$	...	...	$6.0\ 10^{19}$
NGC 4261	E3	L1	41.10	$2.6\ 10^{24}$	NGC 4382	S0$_1$ pec	...	<37.93	$<6.1\ 10^{19}$
NGC 4365	E3	...	38.25	$<3.2\ 10^{19}$	NGC 4383	S0:	MRK star-form.	...	...
NGC 4374	E1	LIN(H); L2	39.50	$2.9\ 10^{23}$	NGC 4435	SB0$_1$	T2/H:; no AGN	38.45	...
NGC 4473	E5	...	<38.14	$<2.2\ 10^{19}$	NGC 4442	SB0$_1$	...	...	$<1.4\ 10^{19}$
NGC 4478	E2	...	<38.49	...	NGC 4474	S0$_1$	...	...	$<1.7\ 10^{19}$
NGC 4486	E0	L2	40.80	$6.9\ 10^{24}$	NGC 4477	SB0$_{1/2}$/SBa	S2	...	$<7.4\ 10^{19}$
NGC 4564	E6	...	38.45	$4.9\ 10^{19}$	NGC 4552	S0$_1$	Comp (W); T2:	39.20	$3.1\ 10^{21}$
NGC 4589	E2	L2	38.90	$2.1\ 10^{21}$	NGC 4649	S0$_1$	...	38.09	$9.4\ 10^{20}$
NGC 4621	E5	...	38.92	$<1.3\ 10^{19}$	NGC 5128	S0+S pec	S2	41.88	$4.4\ 10^{23}$
NGC 4660	E5	...	38.22	$<3.5\ 10^{19}$	NGC 5273	S0/a	S1.5	40.55	$1.1\ 10^{20}$
NGC 4696	E3	LIN(H)	40.00	...	NGC 5631	S0$_3$/Sa	S2/L2:	...	$1.2\ 10^{20}$
NGC 4697	E6	LIN(W)	38.41	$5.2\ 10^{20}$	NGC 5846	S0$_1$	LIN(H); T2	40.80	$1.6\ 10^{21}$
NGC 5011	E2	LIN(W)	...	...	NGC 5898	S0$_{2/3}$	LIN(W)	...	$<1.5\ 10^{20}$
NGC 5018	E4	LLAGN	<39.41	$3.5\ 10^{20}$	NGC 7192	S0$_2$	LIN(W)	...	...
NGC 5044	E0	LIN(H)	39.44	$4.0\ 10^{21}$	NGC 7332	S0$_{2/3}$	IN(Traces)	<39.70	$<9.5\ 10^{19}$
NGC 5077	E3	LIN(H); L1.9	...	$2.8\ 10^{22}$	IC 5063	S0$_3$/Sa	S2	...	...

The optical activity (columns 3 and 8) is derived from Annibali et al. (2010) who use the following notation: LlN = LINER; AGN = AGN like emission; IN = either faint (Traces) or no emission lines; Comp = transition between HII regions and LINERs. W and H indicate weak emission ($EW(H_\alpha + [NII]6584) < 3\text{\AA}$) and strong emission line galaxies, respectively. For the optical activity class, we also use the notation of Ho et al. (1997) in S is for Seyfert, L for LINERS, T for transition objects and H for HII region (: indicate uncertain estimates). The nuclear X-ray luminosity, $L_{X,nuc}$ (columns 4 and 9) and the radio power at 1.4 GHz, $P_{1.4\ GHz}$ (columns 5 and 10), are from Pellegrini (2010) and Brown et al. (2011), respectively.

Table B2. Ellipticals: kinematical and morphological characterization from optical studies

Ident	Morpho. RSA	Gas vs. stars kinematic peculiarities	Morphological peculiarities	Dust-lane morphology
NGC 636	E1	...	...	asymmetric dust distribution (16)
NGC 720	E5	...	Boxy outer isophotes (6)	no dust (13)
NGC 821	E6	SC (4)	...	no dust (9)
NGC 1209	E6	...	X-like struct.; NW linear feature (6)	...
NGC 1297	E2	...	...	dust-lane (a)
NGC 1275	E pec	...	jet	complex patches (18)
NGC 1339	E4	...	...	no dust (10)
NGC 1374	E0	...	...	no dust (10,11)
NGC 1379	E0	...	...	no dust (11)
NGC 1395	E2	...	NW perpend. feature (6); low contr. shells (7)	...
NGC 1399	E1	...	...	no dust (10,11)
NGC 1404	E2	...	...	no dust (11)
NGC 1407	E0	rotat. min. axis (a)	...	no dust (13)
NGC 1426	E4	...	...	no dust(10)
NGC 1427	E5	...	...	no dust (10,11)
NGC 1453	E2	g-d and g-maj t (a)	...	...
NGC 1549	E2	stars rotat. min. axis (0)	shells (7)	...
NGC 1700	E3	CR s-s(1)	...	chaotic dust patches (10)
NGC 2300	E3	...	...	no-dust (10)
NGC 2974	E4	SC(4)	multiple shells (6); g-d and g-maj t≈20° (a)	spiral dust-lanes (10)
NGC 3193	E2	...	...	no dust (9)
NGC 3258	E1	CR g-s (1)	...	no dust (13)
NGC 3268	E2	...	...	small disk of dust (a,16)
NGC 3377	E6	modest star rotat. min. axis (3); SC(4)	...	chaotic dust patches and filam. (9,10)
NGC 3379	E0	SC (4)	...	nuclear dust ring (10)
NGC 3557	E3	...	SW fan; asym. outer isophotes (6)	nuclear ring of dust (10)
NGC 3608	E1	CR s-s (3); KDC (4)	...	nuclear dust ring (10)
NGC 3818	E5	...	...	...
NGC 3904	E2	...	...	...
NGC 3962	E1	...	gas disk+outer arc-like struct. (a)	dust patches (a)
NGC 4261	E3	...	NW tidal arm/ faint SE fan (6)	dust disk (9)
NGC 4365	E3	...	Faint SW fan (6)	no dust (10)
NGC 4374	E1	Rotat. Vel. ≈0 (3); SC (4)	...	dust-lane (a,9)
NGC 4473	E5	complex moprh. of σ and Vel. Field (3); MC (4)	...	no dust (10)
NGC 4478	E2	...	...	no dust (10)
NGC 4486	E0	V≈0 (3); SC(4)	jet	no dust (9)
NGC 4589	E2	...	...	chaotic dust patches (10)
NGC 4564	E6	SC (4)	...	no-dust (9)
NGC 4621	E5	CR s-s inner2″ (3); KDC (4)	...	no dust (10)
NGC 4660	E5	two disk components (3); MC (4)	...	no dust (9)
NGC 4696	E3	...	Faint outer shells (2)	dust arc (a,11,13)
NGC 4697	E6	...	Non spherical inner isophotes (6)	disk (23)
NGC 5011	E2	...	...	no dust (11,13)
NGC 5018	E4	...	multiple tidal tails and shells (6,7)	dust nuclear ring/chaotic (10)
NGC 5044	E0	CR s-s; gas irr.motion (a)	gas fil. shape (a)	chaotic dust patches (15)
NGC 5077	E3	CR s-s (a); g-d and g-maj t≈90° (a)	...	dust filaments (9)
NGC 5090	E2	...	...	no dust (11,13)
NGC 5638	E1	...	...	...
NGC 5812	E0	...	Tidal tail (2)	dust nuclear disk 0.4″ diameter (a)
NGC 5813	E1	CR s-s; gas irr. motion (a); KDC (4)	gas fil. shape (a)	dust nuclear ring/chaotic (10)
NGC 5831	E4	CR s-s (2,3); KDC (4)	...	no dust (9)
NGC 7619	E3	rotat. min. axis (17)	...	no dust (10)
IC 1459	E1	CR g-g (1)	Multiple shells (6)	dust nuclear ring/chaotic (10)
IC 2006	E1	CR g-s (1)	...	...
IC 3370	E2 pec	...	X-like struct.; broad N fan (6); polar ring? (5)	spiral dust-lane (10,11)
IC 4296	E0	CR s-s (a)	...	nuclear ring (10)

In column 3 we use the following notation: **CR g-s**: counter rotation gas vs. stars; **CR s-s**: counter rotation stars vs. stars; **CR g-g**: counter rotation gas vs. gas; **rotat. min. axis**: stars rotate along the galaxy minor axis; **g-d and g-maj t**: gas disk and galaxy major axis are tilted by the reported angle, if provided in the literature. **KDC**: kinematical decoupled component, not necessarily counter-rotation; **MC**: multiple components; **SC** single component (see Krajnović et al. 2008). A description of the kinematic and morphological peculiarities of the galaxies and full references are reported in in Rampazzo et al. (2005) and Annibali et al. (2006) labelled by (a). Further kinematical references: (0) Rampazzo (1988); (1) Corsini et al. (1998); (2) Davies et al. (1983); (3) Emsellem et al. (2004); (4) Krajnović et al. (2008); (5) Sil'chenko et al. (2009) Morphological peculiarities are from: (6) Tal et al. (2009); (7) Malin & Carter (1983); (8) Pierfederici & Rampazzo (2004). The dust detection and structure in the optical bands are from (9) Zhang et al. (2008); (10) Lauer et al. (2005); (11) Sadler & Gerhard (1995); (12) Coccato et al. (2004); (13) Véron-Cetty & Véron (1988); (14) Morganti et al. (2007); (15) Temi et al. (2007); (16) Ferrari et al. (2002); (17) Pu et al. (2010); (18) Tremblay et al. (2007); (19) Wiklind & Henkel (2001); (20) Simões et al. (2007); (21) Pinkney et al. (2003); (22) Patil et al. (2007); (23) van Dokkum & Franx (1995); (24) Kormendy et al. (2009); Whitmore et al. (1990).

Table B3. E/S0s and S0s: kinematical and morphological characterization from optical studies

Ident	Morpho. RSA	Gas vs. stars kinematic peculiarities	Morphological peculiarities	Dust-lane morphology
NGC 1052	E3/S0	CR g-g (1,a)	...	dust (9)
NGC 1351	$S0_1$/E6	...	...	no dust (11)
NGC 4472	E1/$S0_1$	CR s-s (1)	...	chaotic dust patches (10)
NGC 4550	E/S0	CR -ss (1); Slow rot (3); sC (4)	...	asymmetric dust patches (19)
NGC 4570	E7/$S0_1$	MC (4)	...	no dust (20)
NGC 4636	E0/S01(6)	gas irr. motion (a)	...	dust lanes (9)
NGC 5353	$S0_1$/E7	...	...	...
NGC 6868	E3/S02/3(3)	CR g-s (a)	...	dust patches (a,11)
NGC 584	$S0_1$	...	Non-spherical isophotes (6)	chaotic dust patches (10)
NGC 1366	E7/S01(7)	...	...	...
NGC 1389	S01(5)/SB01	...	...	no-dust (11)
NGC 1533	SB02(2)/SBa	...	...	no-dust (11)
NGC 1553	S01/2(5)pec	...	shells (7)	no-dust (13)
NGC 2685	$S0_3$ pec	σ double peak (7); SC (4) gas min.axis grad (12)	polar ring (25)	polar dust lanes (7)
NGC 3245	$S0_1$	...	...	...
NGC 4036	$S0_3$/Sa	gas min.axis grad (12)	...	irr.dust structures (20)
NGC 4339	$S0_{1/2}$	...	...	...
NGC 4371	$SB0_{2/3}$(r)	...	...	dust disk (20)
NGC 4377	$S0_1$	...	...	...
NGC 4382	$S0_1$ pec	CR s-s (3); MC(4)	shells (24)	no dust (10) or weak (20)
NGC 4383	S0:	gas min.axis grad (12)	...	...
NGC 4435	$SB0_1$	...	Interact. with NGC 4438	dust nuclear disk (12)
NGC 4442	$SB0_1$	...	...	...
NGC 4474	$S0_1$	...	...	...
NGC 4477	$SB0_{1/2}$/SBa	CR s-s (1); SC (4)	kin. and phot. axes misaligned (3)	dust spiral (20)
NGC 4552	S01(0)	KDC (4)	shells (7)	chaotic dust patches (10)
NGC 4649	$S0_1$	asym. rot. curve (21)	...	no dust (10)
NGC 5128	S0+S pec	gas min.axis grad (12)	Many shells (7), warps (11)	strong dust lane (11)
NGC 5273	S0/a		...	weak dust features (20)
NGC 5631	$S0_3$/Sa	CR (g-s) (5)	...	...
NGC 5846	$S0_1$(0)	gas irr. motion (a); SC(4)	Faint outer shells (6)	dust filaments extended (a)
NGC 5898	$S0_{2/3}$(0)	CR g-s (1); gas min.axis grad (12)	Three spiral arm-like tidal tails (6)	dust patches (22)
NGC 7192	$S0_2$(0)	CR s-s (a)	Shell (6)	no dust (13)
NGC 7332	$S0_{2/3}$	CR g-g (1); KDC (4); gas min.axis grad (12)	...	...
IC 5063	$S0_3$(3)pec/Sa	gas min.axis grad (12)	...	dust-lane (14)

References and legenda as in Table B2.